Quaternary Science Reviews 325 (2024) 108471

Contents lists available at ScienceDirect

Quaternary Science Reviews

journal homepage: www.elsevier.com/locate/quascirev

Reconstructing the environmental conditions experienced by early modern humans at Tam Pà Ling (northeast Laos) using higher plant wax biomarkers

M.S. McAllister-Hayward [a,*], A.J. Blyth [b], F.A. McInerney [c,d], A.I. Holman [b], K. Grice [b], J.J. Tyler [d], K.W. Westaway [e], R. Joannes-Boyau [f], S. Boualaphane [g], N. Bourgon [h], T.E. Dunn [i], S. Frangeul [j], T. Luangkhoth [g], J.-L. Ponche [k], P. Sichanthongtip [g], V. Souksavatdy [g], E. Suzzoni [j], A. Zachwieja [l], C. Zanolli [m], A.-M. Bacon [n], P. Duringer [o], J.-J. Hublin [p,q], L. Shackelford [r,s], F. Demeter [t,u], M.W. Morley [a]

[a] *Flinders Microarchaeology Laboratory, College of Humanities, Arts and Social Sciences, Flinders University, Adelaide, South Australia, Australia*
[b] *WA-Organic & Isotope Geochemistry Centre, The Institute for Geoscience Research, School of Earth and Planetary Sciences, Curtin University, Perth, Western Australia, Australia*
[c] *School of Earth and Environmental Sciences, University of Queensland, Queensland, Australia*
[d] *School of Physics, Chemistry and Earth Sciences, The University of Adelaide, Adelaide, South Australia*
[e] *School of Natural Sciences, Faculty of Science and Engineering, Macquarie University, Sydney, Australia*
[f] *Geoarchaeology and Archaeology Research Group (GARG), Southern Cross University, Lismore, NSW, Australia*
[g] *Ministry of Information, Culture and Tourism, Vientiane, PDR, Laos*
[h] *IsoTROPIC Research Group, Max Planck Institute of Geoanthropology, Kahlaische Strasse 10, D-07745, Jena, Germany*
[i] *Anatomical Sciences Education Centre, Oregon Health & Sciences University, Portland, OR, USA*
[j] *Spitteurs Pan, Technical Cave Supervision and Exploration, La Chapelle en Vercors, France*
[k] *Université de Strasbourg, Laboratoire Image, Ville Environnement, UMR, 7362, UdS CNRS, Strasbourg, France*
[l] *Department of Biomedical Sciences, University of Minnesota Medical School, Duluth, MN, USA*
[m] *Univ. Bourdeaux, CNRS, MCC, PACEA, UMR 5199, F-33600, Pessac, France*
[n] *Université Paris Cité, CNRS, BABEL, UMR 8045, 75012, Paris, France*
[o] *Ecole et Observatoire des Sciences de La Terre, Institut de Physique du Globe de Strasbourg (IPGS), UMR 7516, CRNS, Université de Strasbourg, Strasbourg, France*
[p] *Chaire de Paléoanthropologie, CIRB (UMR 7214-U1050), Collège de France, 11 Place Marcelin-Berthelot, 75231, Paris, Cedex 05, France*
[q] *Max Planck Institute for Evolutionary Anthropology, Deutscher Platz 6, Leipzig, Germany*
[r] *Department of Anthropology, University of Illinois at Urbana-Champaign, Urbana, IL, USA*
[s] *Carle Illinois College of Medicine, University of Illinois at Urbana-Champaign, Urbana, IL, USA*
[t] *Lundbeck Foundation GeoGenetics Centre, Globe Institute, University of Copenhagen, Copenhagen, Denmark*
[u] *Eco-anthropologie (EA), Dpt ABBA, Muséum National d'Histoire Naturelle, CNRS, Université Paris Cité, Musée de L'Homme, Paris, France*

ARTICLE INFO

Handling Editor: Dr P Rioual

Keywords:
n-alkanes
n-alkanols
stable isotopes
palaeoenvironments
Homo sapiens

ABSTRACT

The sediments of Tam Pà Ling (TPL), northeastern Laos, have yielded the earliest evidence of *Homo sapiens* in mainland Southeast Asia (~86 ka; marine isotope stage (MIS) 5 b) with a number of skeletal elements having been recovered from the sequence attesting to two populations of *H. sapiens* present in the vicinity between 77 ± 9 ka to 39 ± 9 ka. At present there has been very limited research into the environmental conditions that these populations encountered during MIS 5–4. In this study, we present the results of an analysis of higher plant biomarkers (*n*-alkanes and *n*-alkanols) from the sediments at TPL to reconstruct the palaeovegetation of the site and the human fossils. The *n*-alkane $\delta^{13}C$ values demonstrate that *H. sapiens* encountered a predominantly C_3 forest landscape in MIS 5 b-MIS 4 that prevailed until MIS 1. Observations of a fluctuation in $\delta^{13}C$ values across MIS 5 b-MIS 1 (~86–3 ka) indicates that moisture availability was non-uniform, most likely resulting in landscape changes in and around TPL. The presence of *H. sapiens* at TPL during the environmental conditions associated with MIS 5 b-MIS 3 highlights the adaptability of our species to environmental dynamics at this time.

* Corresponding author.
E-mail address: meghan.mcallister@flinders.edu.au (M.S. McAllister-Hayward).

https://doi.org/10.1016/j.quascirev.2023.108471
Received 22 August 2023; Received in revised form 6 December 2023; Accepted 12 December 2023
Available online 12 January 2024

1. Introduction

The first presence of *Homo sapiens* in mainland Southeast Asia (MSEA) has recently been extended back to 77 ± 9 ka, close to the final stages of Marine Isotope Stage (MIS) 5 (Freidline et al., 2023). Uncertainty still remains, however, regarding the exact time of arrival, migration routes and settlement patterns of early humans in this region (Bae et al., 2017; Boivin et al., 2013; Bradshaw et al., 2021; Roberts et al., 2015a; Reyes-Centeno, 2016). The extent to which climatic and environmental conditions influenced the dispersal of our species into new regions is also hotly debated (Bird et al., 2005; McAllister et al., 2022 *and references therein*), and this is in part confounded by the relatively limited number of palaeoenvironmental studies with which to compare to data emerging from Late Pleistocene archaeological sites.

New research from the Tam Pà Ling (TPL) Cave, Laos, has documented the earliest evidence for *H. sapiens* in MSEA (Demeter et al., 2012, 2015, 2017; Freidline et al., 2023; Shackelford et al., 2018). A partial cranium (TPL1), two mandibles (TPL2, TPL3), a rib (TPL4), a pedal phalanx (TPL5), a frontal bone (TPL6) and a tibial fragment (TPL7) have been recovered from sediments ranging from 77 ± 9 ka to 39 ± 9 (Freidline et al., 2023). This evidence demonstrates that *H. sapiens* were present in and around the site intermittently over a period of ~56 kyr, from the end of MIS 5 (the upper age limit of the oldest dated sample from TPL is ~86 ka) (Freidline et al., 2023). In island Southeast Asia (ISEA), Lida Ajer, Sumatra currently holds the earliest evidence of *H. sapiens*, with their presence dating back to at least 73 ka (Louys et al., 2022; Westaway et al., 2017). These early finds are challenging the once conventional belief that *H. sapiens* left Africa moving eastwards into Southeast Asia and beyond to Australia following a coastal route from around 60–50 ka (O'Connell et al., 2018).

Research has demonstrated that changes in environmental and ecological conditions had a profound impact on the adaptive plasticity of hominins and other megafauna in Southeast Asia during the Quaternary (Louys and Roberts, 2020; Rizal et al., 2020; Sutikna et al., 2016). Marked environmental changes are thought to have led to the decline of various hominins (e.g., *Homo erectus*) as they are believed to have been primarily adapted to open landscapes, often in close proximity to rivers and lakes (Bettis et al., 2009; Gamble, 1993, 2013; Louys and Roberts, 2020; Roberts and Stewart, 2018). While *H. erectus* and other co-existing hominins demonstrated technological complexities and social networks (Joordens et al., 2016; Langley et al., 2008; Zilhão, 2012), as well as being capable of living around forested environments, their reliance on grassland and woodland environments would have put them at a disadvantage to *H. sapiens* in forested environments (Roberts and Stewart, 2018). This question was also raised for Denisovans in northern Laos (Demeter et al., 2022), which occupied ecosystems composed of predominantly open landscapes (Bacon et al., 2023). The continental scale shift in the Middle and Late Pleistocene resulted in an expansion of dense forested landscapes, with the decline and eventual extinction of these archaic species being attributed to their inability to adapt to these changes and compete with the 'generalist specialist' *H. sapiens* (Bacon et al., 2023; Louys and Roberts, 2020; Roberts and Stewart, 2018). Therefore, determining the palaeovegetation conditions experienced by early *H. sapiens* during the Late Pleistocene is imperative to better comprehend the adaptability of our species, allowing researchers to better connect changes in the landscape with evolutionary and cultural changes.

To improve understandings of the extent to which environmental conditions influenced the movements and behaviours of *H. sapiens*, local palaeoenvironmental (i.e., palaeoevegetation and palaeohydrology) reconstructions generated from the analysis of appropriate materials recovered from archaeological sites are required. At TPL, Milano et al. (2018) analysed the stable carbon ($\delta^{13}C$) and oxygen ($\delta^{18}O$) isotopes from the terrestrial gastropod *Camaena massiei* and inferred that the environment was largely humid and forested until the Last Glacial Maximum (LGM). Analysing the $\delta^{13}C$ values of two teeth from TPL1 (63–46 ka), Bourgon et al. (2021) also found values (−26.4‰) to fall within the ranges expected of a C_3 forested environment prior to the LGM. During the LGM, Milano et al. (2018) inferred a climatic shift to drier conditions, resulting in the expansion of open landscapes. However, this record is complicated by low sample resolution (there is only one *C. massiei* recovered for the earliest 16 kyr period (78–62 ka)), an issue exacerbated by the recent expansion of the sediment chronology by Freidline et al. (2023). Further proxy records are clearly required to develop a comprehensive understanding of the local palaeovegetation at TPL.

Biomarkers (molecular fossils) originating from natural products within eukaryotes, archaea and bacteria can provide potentially valuable insights into past environmental change, including those from archaeological deposits (Patalano et al., 2021). The cuticle of terrestrial higher plants is coated with protective waxes (Eglinton and Hamilton, 1967) comprised of a mixture of long chain aliphatic *n*-alkyl derivatives: normal alkanes (*n*-alkanes), *n*-alkanols, *n*-alkanoic acids, triterpenoids and secondary metabolites (Eglinton et al., 1962; Eglinton and Hamilton, 1967; Eiserbeck et al., 2012; Jetter et al., 2006; Schuster et al., 2016). Long-chain (C_{27} to C_{35}) *n*-alkanes have proven to be valuable biomarkers of plants, as their straight-chain hydrocarbon structure enables them to preserve well within marine, lacustrine and terrestrial fossil records (Diefendorf et al., 2011; Smith et al., 2007).

Terrestrial higher plants yield homologous series of *n*-alkanes, typically ranging between C_{27}–C_{35}, often with an odd-over-even chain length predominance (Eglinton et al., 1962; Eglinton and Hamilton, 1967). Although they generally remain unaltered by microbial and diagenetic processes, their preservation is not guaranteed (Logan et al., 1993). Factors that can influence how well *n*-alkanes are preserved in the sediment, if at all, include the level of microbial activity, soil pH, temperature, moisture and oxygen content (Grimalt et al., 1988; Nguyen et al., 2017; Nie et al., 2014; Zech et al., 2011).

It has only been in the last decade or so that the analysis of plant wax biomarkers has been incorporated into archaeological studies as a means to reconstruct the palaeovegetation and palaeohydrological conditions experienced by hominins/early humans and to better understand past human-environment interactions (Patalano et al., 2021). As many archaeological cave sediments in the tropics are characterised by highly oxic conditions, these often compromise the preservation of pollen and subsequently palynological reconstructions (Rabett et al., 2017), whereas in some cases plant biomarkers remain.

To date, there has only been a single application of plant biomarkers to an archaeological site in Southeast Asia. Rabett et al. (2017) successfully extracted and analysed the chain length distribution and $\delta^{13}C$ of leaf wax *n*-alkanes and *n*-alkanoic acids from Hang Trông cave in the Tràng An massif, northern Vietnam. Rabett et al. (2017) found the C_{31} *n*-alkane to dominate, coupled with $\delta^{13}C$ values between −35‰ and −30‰. These results provided strong evidence for an environment dominated by C_3 vegetation during MIS 2 (29 ka) and persisting through the LGM (26–19 ka), similar to the C_3 dominated landscape there today. Expanding the palaeorecord by applying stable carbon isotopes to fossil plant wax *n*-alkanes and *n*-alkanols in Southeast Asia will contribute to a more robust reconstruction and understanding of vegetation and climate changes across the region.

In this study, we analysed relative abundances and $\delta^{13}C$ values of higher plant biomarkers in sediments from TPL. In particular, we examined variability in the concentration of long chain *n*-alkanes and *n*-alkanols to distinguish their higher plant origins and utilise the $\delta^{13}C$ of *n*-alkane and *n*-alkanol biomarkers to reconstruct the local palaeovegetation dynamics of TPL from MIS 5 b-MIS 1. In doing so, we seek to determine if *H. sapiens* encountered a predominantly C_3 vegetated landscape when they were first present in and around the site and if there are variations in the vegetation composition preserved in the sediment record through time. In addition, this study seeks to determine if *H. sapiens* were present at the site during similar environmental conditions.

1.1. Plant wax biomarkers as environmental proxies

1.1.1. $\delta^{13}C$ of n-alkanes

Compound specific isotope analysis (CSIA) of the stable carbon ($\delta^{13}C$) isotope ratios of leaf wax *n*-alkanes reflects the influences of both environmental factors (i.e., atmospheric CO_2 levels, water availability and altitude) (Diefendorf et al., 2010; Farquhar et al., 1989) and biological characteristics (i.e., physiology, genetics and photosynthetic pathway) (Diefendorf and Freimuth, 2017). However, the predominant factor influencing the $\delta^{13}C$ of sedimentary *n*-alkanes is the actual photosynthetic pathway used by a plant to fix CO_2 into its biochemicals (Bi et al., 2005; Collister et al., 1994; Diefendorf and Freimuth, 2017; Zhou et al., 2010). C_4 plants (tropical and sub-tropical grasses and arid-adapted shrubs) are more efficient in their assimilation of carbon and have grown to dominate arid and/or semi-arid regions with warmer and drier conditions, as well as areas characterised by warm-season rainfall (Tipple and Pagani, 2007). The $\delta^{13}C$ values of these *n*-alkanes largely fall between −25‰ and −18‰ (Bi et al., 2005; Collister et al., 1994; Liu and An, 2020; Sage, 2017). C_3 plants, which includes nearly all trees, most shrubs and temperate grasses, tend to dominate in cooler and/or wetter environments (Diefendorf et al., 2010; Lloyd and Farquhar, 1994). C_3 plants are much less efficient in the assimilation of carbon and have notably lower *n*-alkane $\delta^{13}C$ values than C_4 plants, ranging between −39‰ and −27‰ (Bi et al., 2005; Collister et al., 1994; Liu and An, 2020). CAM photosynthesising plants are not discussed here as they are largely restricted to arid areas (Edwards, 2019; Silvera et al., 2010; Still et al., 2003) and are highly unlikely to be present in tropical and sub-tropical regions.

Any study examining *n*-alkanes preserved in sediments (e.g., Rabett et al., 2017 from Tràng An, Vietnam; Patalano et al., 2023 from Lesotho, Africa) analyses an aggregate compound pool derived from many plants in the environment. It is therefore possible to use the $\delta^{13}C$ values of sedimentary *n*-alkanes to infer the proportion of C_3 versus C_4 plants present within the landscape at different time periods. However, isotope variation can occur within one photosynthetic group. In dense woodland, changes in the $\delta^{13}C$ values of C_3 trees are predominantly interpreted to reflect the 'Canopy Effect'- a decline in the $\delta^{13}C$ values of leaves from the top of the canopy to the forest floor (Vogel, 1978) - and variations in moisture availability (Farquhar et al., 1989; Medina and Minchin, 1980; van der Merwe and Medina, 1991). Photosynthesising plants in the upper canopy have greater exposure to sunlight (irradiance) and lower humidity levels, which leads to an increase in $\delta^{13}C$ values, whereas those in the more shaded under canopy, experience greater discrimination against ^{13}C, hence lower $\delta^{13}C$ (Farquhar et al., 1989; Graham et al., 2014; van der Merwe and Medina, 1991). Further declines in the $\delta^{13}C$ of vegetation photosynthesising on or near the forest floor can also be explained by the uptake of recycled ^{13}C depleted CO_2 produced by soil respiration (Medina and Minchin, 1980; Vogel, 1978).

In the tropics and subtropics, annual variability in moisture availability is an additional and important factor affecting the $\delta^{13}C$ values of *n*-alkanes from C_3 plants. Precipitation patterns in the tropics and subtropics of Southeast Asia are largely dictated by the Asian Monsoon, with the majority of rainfall falling during the summer monsoon (Chiang et al., 2020; Webster et al., 1998). During extended periods of lower precipitation during winter, C_3 vegetation becomes water stressed, leading to an increase in water use efficiency and a corresponding decrease in carbon isotope fractionation and stomatal conductance, causing increased $\delta^{13}C$ values (Diefendorf and Freimuth, 2017; Farquhar et al., 1989). When the summer monsoon patterns are weakened and the winter monsoon is strengthened over an extended period of time (e.g., during cooler/glacial conditions; the LGM), this can result in a rise of areas/patches of open landscapes in the forest canopy (e.g., Milano et al., 2018; Suraprasit et al., 2021). However, during the earlier cooler (MIS 6, MIS 4) and warmer (MIS 5) periods Bacon et al. (2021) observed the $\delta^{13}C$ and $\delta^{18}O$ values of mammalian fauna from northern Vietnam (Coc Muoi and Duoi U'Oi) and northeastern Laos (Tam Hang South and Nam Lot) to suggest an opposite effect. They found temperate C_3 forests to dominate towards the end of MIS 6 and in MIS 4, whereas MIS 5 was characterised by more diverse vegetation, consisting of rainforests and intermediate forests with areas of open landscape.

1.1.2. n-Alkanols

Similar to long chain *n*-alkanes, long chain *n*-alkanols (C_{24}–C_{34}) can also be used to distinguish the plant functional type and photosynthetic pathway of palaeovegetation through ACL and CSIA, respectively (Chikaraishi & Naraoka, 2007; Diefendorf et al., 2011; Rommerskirchen et al., 2003, 2006; Vogts et al., 2009). Unlike *n*-alkanes, long chain *n*-alkanols from vascular higher plants possess a strong even-over-odd carbon predominance (Eglinton and Hamilton, 1967). The *n*-C_{26}, *n*-C_{28} and *n*-C_{30} alkanols are often preferentially produced by dicots (woody taxa, trees, and shrubs), whereas the longer chain *n*-C_{32} *n*-alkanols are more abundant in graminoids (grasses), with their $\delta^{13}C$ ranges also largely aligning with those of C_3 and C_4 *n*-alkanes (Rommerskirchen et al., 2006; Vogts et al., 2009). The $\delta^{13}C$ values of *n*-alkanols are also analysed in this study to assess if they complement the $\delta^{13}C$ *n*-alkane record, as demonstrated by Vogts et al. (2009). If there are variations in $\delta^{13}C$ values between *n*-alkanes and *n*-alkanols, the potential factors that may have led to these differences are discussed.

2. Materials & methods

2.1. Study site: Tam Pà Ling, northeastern Laos

Laos (14–20°N) lies across the Tropic of Cancer and has an average annual temperature of 21.5 °C, ranging between a minimum of 15.7 °C in December and a maximum of 25.3 °C in June and July (Milano et al., 2018). Precipitation patterns are largely controlled by the Asian Monsoon (of which the Indian and East Asian Monsoons are subsystems), with variations in monsoon dynamics creating significant variations in rainfall (Thomson et al., 2021; Webster et al., 1998). Averaged between 1910-2017 (weatherbase.com), annual precipitation in the region is 1903 mm, ranging from 51 mm during the winter monsoon (dry season) from November–April and increasing to 267 mm during the summer monsoon (wet season) from May–October (Milano et al., 2018). The relative humidity is consistently high, averaging 80.5% and ranging between 77.6% during the dry season and 83.4% in the wet season (Milano et al., 2018).

Using remote sensing data, Milano et al. (2018) found 66.4% of the vegetation surrounding TPL was woody plants (C_3), with 28.4% comprising of grasslands and shrubs (C_4) and the remaining 5.2% consisting of artificial infrastructures. Not including infrastructure, Milano et al. (2018) found the modern vegetation of TPL to be predominantly comprised of C_3 vegetation (70.1%), interspersed with C_4 vegetation (26.3%). Li and Yang (2022) described the vegetation to be predominantly comprised of tropical montane (mixture of deciduous trees and gymnosperms, with shrubs and ferns present in abundance), tropical monsoon (characterised by oak trees and shrubs) and deciduous forests, with many of these forests dominated by Teak.

TPL is located in Huà Pan Province, northeastern Laos, ~260 km NNE of Vientiane (20°12′31.4″N, 103°24′35.2″E), situated at the top of Pà Hang Hill, at an elevation of 1170 m (Demeter et al., 2012). The cave lies within the Annamite Mountain Range, characterised by Upper Carboniferous to Permian limestone beds, limestone karsts, sinkholes, towers, caves and caverns (Duringer et al., 2012). Whilst published research on the region dates back to the 1930s, following excavations of Tam Hang by geologist Jacques Fromaget (Fromaget, 1936, 1937, 1940), TPL remained unstudied until 2008, with excavations commencing from 2009 (Demeter et al., 2012, 2015, 2017; Freidline et al., 2023; Shackelford et al., 2018).

The cave is accessed through a single south-facing entrance (Fig. 1). The main chamber is located 65 m below the entrance and measures 40 m wide, 30 m long and 12 m high (Fig. 1) (Demeter et al., 2012). The

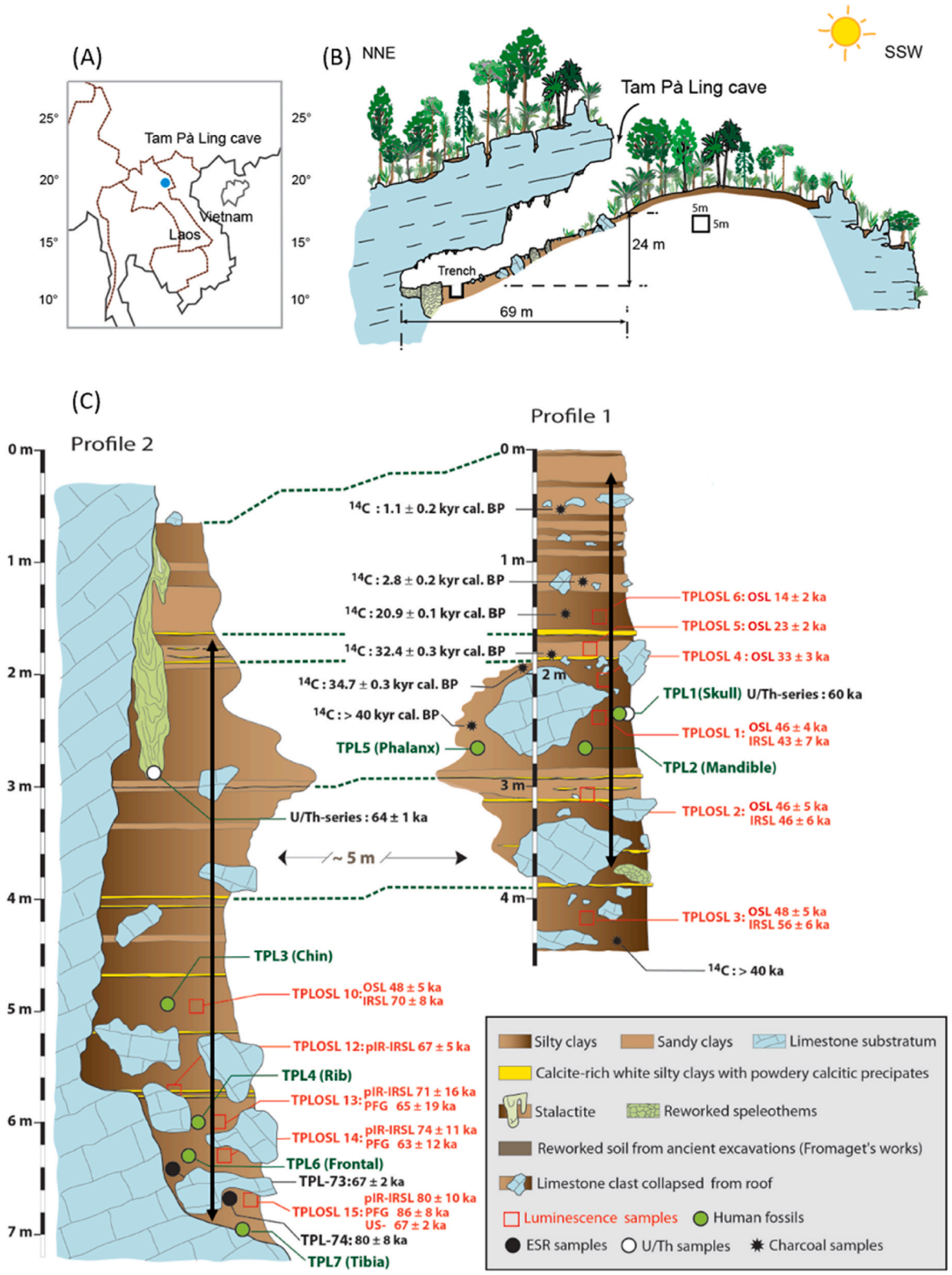

Fig. 1. (A) Location of Tam Pà Ling, (B) Section of Pà Hang Mountain showing the location of Tam Pà Ling, and (C) Stratigraphy and current chronology of Tam Pà Ling (redrawn from Freidline et al., 2023). Arrows through P1 from 0.2 m to 3.7 m and P2 from 1.67 m to 6.92 m illustrate the depths spanned by sediment samples collected in this study. Location of vertical black arrows do not represent exact locations samples were excavated from, just depths.

excavated trench currently measures 12 m × 4 m, excavated to depths of 4.5 m (profile 1) and 7 m (profile 2), which are 5 m apart from one another (Freidline et al., 2023; Shackelford et al., 2018). Research presented in this paper is based on the analyses of 45 sediment samples, 18 of which are from profile 1 (P1) and 27 from profile 2 (P2). Stratigraphic layers are dominated by alternating layers of brown sandy and silty clays, punctuated by 12 calcareous layers of powdered calcite precipitate (moonmilk) (Demeter et al., 2012, 2015). Some of these have

locally hard calcite cementation of about 1–2 cm thick, but their lateral extension does not exceed 60 cm.

The cave sediments are sourced from the argillaceous bank around the cave entrance and transported into the cave via slope wash episodes (Demeter et al., 2012, 2015). Upon deposition in the main chamber, excavations and subsequent analyses have demonstrated no evidence of subsequent bioturbation, reworking, mixing or post depositional modifications (Freidline et al., 2023). Further details about the site formation processes and sediment stratigraphy can be found in Demeter et al. (2012, 2015, 2017) and Freidline et al. (2023 *SI*).

2.2. Sample collection and preparations

Eighteen sediment samples extending from 0.2 to 3.7 m from P1 and 27 sediment samples from 1.67 to 6.92 m from P2 were collected as bulk sediment samples from TPL in 2018. Samples were stored in sealed sample bags in Flinders University Archaeology laboratory at room temperature (21 °C) prior to preparation for isotopic and lipid biomarker analyses.

Sediment samples were sieved through a 2-μm mesh to remove all non-sediment materials (bone, shell fragments, rocks). The sieve was cleaned with Triple 7 EnviroLab LabPower, with 3 rinses in water, ethanol, deionised water and acetone between each sample. Samples were dried in a LabTech Forced Convection Oven LDO-150 F at 30 °C (72 h). Remaining sample preparation and data analyses (except bulk sediment $\delta^{13}C$) were conducted at the Western Australian Organic & Isotope Geochemistry Centre (WA-OIGC), Curtin University. Samples were freeze dried in an ALPHA 1–2 LDplus freeze-drier (24 h) and homogenised in a Rocklabs Benchtop Ring Mill with a zirconia head (30 s mill time).

2.3. Bulk organic $\delta^{13}C$ analysis

Sediment samples (~1 g) were acidified in 10% concentrated HCl for 48 h to remove inorganic carbon contents and rinsed three times in deionised water prior to re-drying. Samples (15 mg) were analysed for carbon isotopes in bulk organic matter ($\delta^{13}C_{org}$) on a VarioIsotope Cube (Elementar) coupled to an Isoprime IRMS (GV instruments) at Flinders Analytical, Flinders University. The combustion tube was set to 650 °C and the reduction tube was set to 900 °C. Standards used were L-glutamic acid (USGS 40 and USGS 41a). Drift correction was performed using a series of standards (USGS 40) analysed at the beginning and end of the run. Precision of measurement was reported at 0.1‰.

2.4. Total lipid extraction

Total lipids were extracted from between 10.16 g and 26.28 g of sediment using a Milestone Start E Microwave Extraction System (MES). Samples were prepared in Teflon vessels with DCM:methanol 9:1 (50 mL:5 mL). The MES was heated from room temperature to 80 °C (over 10 min) and held at 80 °C (15 min). All utensils used to prepare the sediment samples were cleaned thoroughly and rinsed (3 times each with methanol, DCM and *n*-hexane).

Following extraction, samples were centrifuged in an Eppendorf Centrifuge 5810 (3 min at 1600 rpm) to separate the solvent containing the total lipid extract (TLE) from sediment. The TLE was transferred into pre-cleaned glass vials. Copper turnings were added and left overnight on a Dionex SE 500 evaporator/shaker to remove any elemental sulfur. Samples were concentrated under nitrogen gas (N_2) through the Dionex SE 500 to ~2 mL volume. Samples were then filtered through finely ground magnesium sulphate ($MgSO_4$) to remove the remaining water and fine sediment particles.

The TLE was again concentrated via complete evaporation under N_2 and transferred using 0.5 mL DCM to be adsorbed onto silica gel in a separate 5 mL glass beaker ahead of separation into three fractions (saturated, aromatic and polars) via silica gel chromatography. Chromatography was conducted using 5.5 cm of solvent-cleaned and oven-activated (160 °C) silica gel in a Pasteur pipette. Saturates were separated first, using 2 mL of *n*-hexane, aromatics were then extracted using a 7:3 ratio of *n*-hexane to DCM (1.4 mL *n*-hexane, 0.6 mL DCM) and finally the polar compounds were removed via 1:1 (1 mL of each) of DCM:Methanol.

2.5. n-Alkane analysis

n-Alkanes (C_{14}–C_{35}) in the saturated fraction were identified on an Agilent 7890 B Gas Chromatograph (GC), interfaced to an 5977 B Mass-Selective Detector (MSD) at WA-OIGC at Curtin University. Analysis was conducted using a DB-1 ms ultra-inlet column (60 m × 0.25 mm internal diameter x 0.25 μm film thickness). The split/splitless inlet was operated in pulsed splitless mode at 280 °C. Helium (He) carrier gas was injected at 1.1 mL/min. The GC oven was programmed to hold at 40 °C for 1 min, heat to 325 °C at 3 °C min^{-1} and hold at 320 °C for 30 min. The MSD was operated at 70eV and held at 320 °C. Data was collected in full scan mode from *m/z* 50 to 550. Performance of the GC-MSD was evaluated using a mixture of standards, including *n*-alkanes from C_{10} to C_{35} as well as a range of branched and cyclic alkanes, aromatics, alcohols and fatty acids. The mixture of standards was analysed multiple times per week to assess performance of the instrument and ensure that peak responses were consistent throughout the analyses. Data were analysed with Agilent ChemStation software. Compounds were identified by comparison of mass spectra with commercial library data (NIST mass spectral libraries).

The ACL of *n*-alkanes (C_{14}–C_{35}) and *n*-alkanols (C_7–C_{32}) (Fig. S1) were calculated from the area of each carbon numbered (C_n) *n*-alkyl peak from the total ion chromatograms using the following equation:

$$\mathrm{ACL} = \frac{\sum(Cn \times area)}{\sum area} \quad (1)$$

The carbon preference index (CPI) was also calculated for long chain *n*-alkanes (C_{27}–C_{35}) and *n*-alkanols (C_{26}–C_{32}) using equations (2) and (3), respectively, adapted from Marzi et al. (1993) to distinguish their sources. CPI values > 1 indicate terrestrial plant origins, whereas values < 1 represent petrogenic, anthropogenic or bacterial inputs (Bray and Evans, 1961; Eglinton and Hamilton, 1967; Rommerskirchen et al., 2003).

$$\mathrm{CPI} = \frac{[\Sigma_{odd}(C_{27} - C_{33}) + \Sigma_{odd}(C_{29} - C_{35})]}{(2\Sigma_{even}C_{26} - C_{34})} \quad (2)$$

$$\mathrm{CPI} = \frac{[\Sigma_{even}(C_{26} - C_{30}) + \Sigma_{even}(C_{28} - C_{32})]}{(2\Sigma_{odd}C_{27} - C_{31})} \quad (3)$$

2.6. Plant wax n-alkane $\delta^{13}C$ analysis

The $\delta^{13}C$ values of the *n*-alkanes were measured with a Gas Chromatography-Isotope Ratio Mass Spectrometer (GC-irMS) at WA-OIGC, using a Thermo Trace GC Ultra with GC Isolink, connected to a Delta V Advantage irMS via Conflo IV. Analysis was conducted using a DB-1 ms ultra-inlet column (60 m × 0.25 mm internal diameter x 0.25 μm film thickness). The split/splitless inlet was operated in pulsed splitless mode at 280 °C. Helium (He) carrier gas was injected at 1.5 mL/min. The oven temperature held at 40 °C for 1 min, heating to 325 °C at 3 °C/min, holding this for 30 min. The outflow from the GC column passed through the GC Isolink combustion furnace (packed with copper oxide and nickle oxide, held at 1000 °C) to combust the hydrocarbons to CO_2. The CO_2 travelled through the Conflo IV into the irMS, which measured the *m/z* for CO_2 at 44, 45 and 46. Each sample was run in triplicate and $\delta^{13}C$ values were calculated from the measured masses via Thermo Isodat software. Values were normalised to the international VDPB scale through a comparison with an in-house mixture of *n*-alkane standards (*n*-C_{11}, *n*-C_{13}, *n*-C_{14}, *n*-C_{17}, *n*-C_{18}, *n*-C_{19} and *n*-C_{25}) of known

isotopic composition (δ^{13}C between −32.2‰ and −25.3‰). Triplicate values had a standard deviation of less than 0.5‰.

2.7. Polar compound identification

Following chromatic separation, the polar compounds were evaporated under N_2 and weighed. Polar compounds were derivatised via the formation of trimethylsilyl ethers by adding 10 μL each of pyridine and BSTFA per 0.5 mg of polar sample and placing these on a hotplate at 60 °C (20 min). *n*-alkanols (C_7–C_{32}) of the polar fraction were identified on an Agilent 6890 N GC, coupled to a 5975 B MSD, using an Agilent DB-5MS UI column. Column dimensions and the oven program remained the same as for the saturated compounds, detailed in 2.5, with data analysed in Agilent ChemStation software.

2.8. Polar $\delta^{13}C$ analysis

δ^{13}C values of the polar compounds were measured on a GC-irMS, using the Thermo Trace GC Ultra with GC Isolink, connected to a Delta V Advantage irMS via Conflo IV. Analysis was conducted under the same conditions as detailed for the saturated fractions, with the exception of using an Agilent DB-5MS UI GC column instead of a DB-1 ms ultra-inlet column. To correct for the influence of the derivatisation agent on the isotopic values, the method and equation presented in Rieley (1994) were applied:

$$n_{xd} \times \delta_{xd} = (n_x \times \delta_x) + (n_d \times \delta_d) \quad (4)$$

Where *x* represents the underivatised compound, *d* the derivatised reagent, *xd* the derivatised compound, δ the isotope value of each, and *n* the number of carbon atoms in each. To calculate the δ value of the derivatisation reagent (δ_d), a cholesterol standard was run both underivatised (−21.99‰) and derivatised (−23.03‰). Cholesterol has 27 carbon atoms, with BSTFA adding 3 more carbon atoms. δ_d is calculated to be −32.37‰. The δ_d is used to calculate the δ value of the underivatised compounds (provided the same batch of derivatisation reagent is used) by rearranging equation (4):

$$\delta_x = \frac{(n_{xd} \times \delta_{xd}) - (n_d \times \delta_d)}{n_x} \quad (5)$$

3. Results

δ^{13}C values for sediment samples collected at 0.2 m, 0.3 m, 0.4 m, 6.72 m and 6.92 m (Fig. S3) are omitted from Figs. 2–4 as they are from depths above and below the youngest and oldest dated sediment samples (Table S1). Interpolated ages and age errors were inferred from 2σ modelled age boundaries from Freidline et al. (2023), presented in Table S1, by linear interpolation between bracketing ages in R (version 4.3.2). The Bayesian age model developed using OxCal v4.4 for TPL is presented in Fig. 5 of Freidline et al. (2023), for reference. Dates were not extrapolated above and below the youngest and oldest dates due to uncertainties about the potential ages of undated samples above and below the established chronology. Error bars are not included in the aforementioned figures as they hinder the illustration of trends through time, the age errors are presented in Table S1. The impact of the large age errors (ranging from ±1882 to ±8444 years) for interpolated ages on interpretations through time is addressed in the discussion.

3.1. n-Alkyl CPI

n-alkane CPI values range between 10.2 and 0.5 (Fig. 2, Tables S3 and S4). The 5 of the 45 sediments samples (all from P2) that returned CPI values < 1 (falling under the vertical dashed line in Fig. 2), are omitted from figures and interpretations, as they are unlikely to have originated from terrestrial higher plants. CPI values of *n*-alkanols range from 8.6 to 3.7, indicating terrestrial plant origins.

3.2. Plant wax n-alkane $\delta^{13}C$

Plant wax *n*-alkane δ^{13}C measurements of the 45 sediment samples are presented for *n*-alkanes C_{27} to C_{33} (see Tables S5 and S6). The δ^{13}C

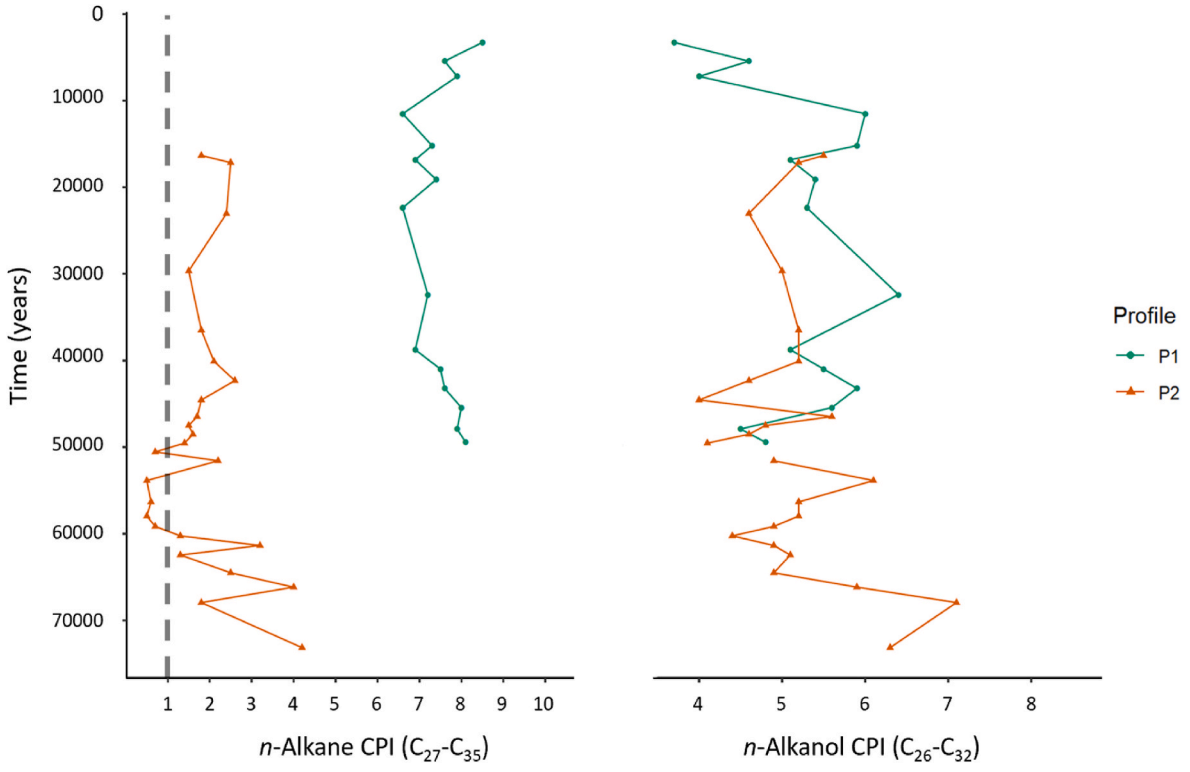

Fig. 2. Long chain (C_{27}–C_{35}) *n*-alkane CPI (left) plotted alongside the long chain (C_{26}–C_{32}) *n*-alkanol CPI. These are plotted against linearly interpolated ages.

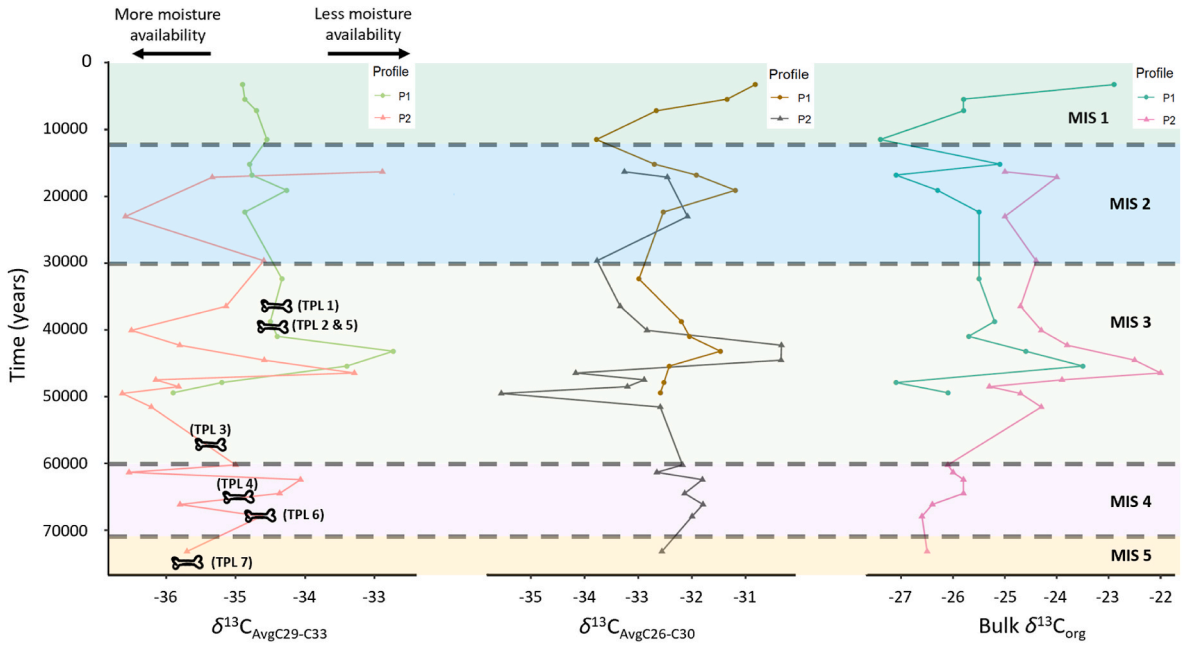

Fig. 3. The weighted average of the three dominant *n*-alkanes ($\delta^{13}C_{AvgC29-C33}$) *n*-alkanols ($\delta^{13}C_{AvgC26-C30}$) and bulk $\delta^{13}C_{org}$ plotted against time (years). Bones plotted on $\delta^{13}C_{AvgC29-C33}$ represent *H. sapiens* fossils from TPL. Fossils have not been directly dated and are presented at approximate ages based on the interpolated ages from the sediment profiles they were recovered from.

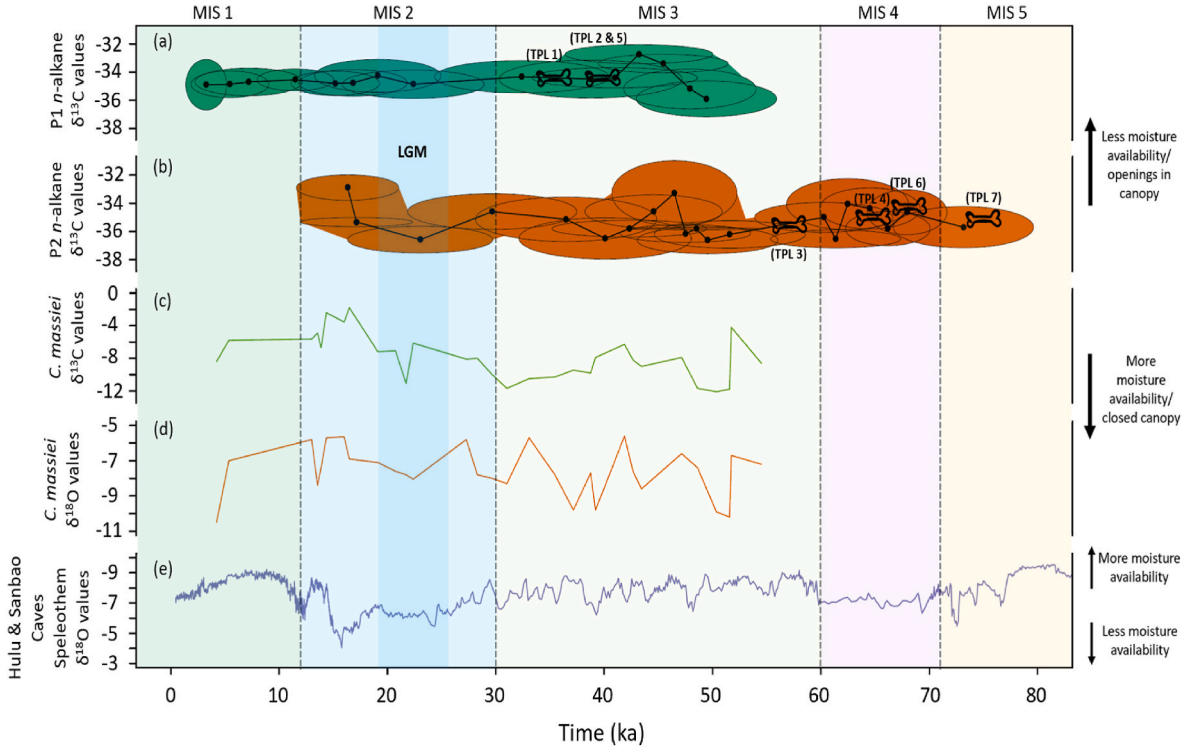

Fig. 4. (a) TPL *n*-alkane $\delta^{13}C_{AvgC29-C33}$ values from P1, (b) TPL *n*-alkane $\delta^{13}C_{AvgC29-C33}$ values from P2, (c) TPL *Camaena massiei* $\delta^{13}C$ values from Milano et al. (2018), (d) TPL *Camaena massiei* $\delta^{18}O$ values from Milano et al. (2018) and (e) $\delta^{18}O$ of speleothems from Hulu and Sanbao Caves, China (Caballero-Gill et al., 2012; Cheng et al., 2009; Wang et al., 2008). Ovals around each data point in (a) and (b) represent errors in time and $\delta^{13}C_{AvgC29-C33}$ values, which is the standard deviation of the $\delta^{13}C$ values of C_{29}, C_{31} and C_{33}. Bones presented on (a) and (b) represent where *H. sapiens* fossils were recovered from P1 and P2. Samples from Milano et al. (2018) which has more than one sample from the same depth are presented as an average value (Table S2).

values of the three dominant homologues C_{29}, C_{31} and C_{33} are presented in Fig. S4. The *n*-alkane weighted average, which is the mean value for the $\delta^{13}C$ values of C_{29}, C_{31} and C_{33} ($\delta^{13}C_{AvgC29-C33}$), is presented in Fig. 3. Only trends observed across all homologues are interpreted in the discussion. The shifts in $\delta^{13}C$ values are large compared to the standard deviations of replicate measurements (Tables S5 and S6) and are therefore likely reflecting true changes in the environment. $\delta^{13}C$ values of *n*-alkanes C_{29}–C_{33} generally decrease with increasing chain length

(Fig. S4). This ^{13}C-depletion with increasing chain length has also been observed in modern plants (Collister et al., 1994).

δ^{13}C variability is greater in all homologues in P2 than in P1 (Tables S5 and S6). Minimum and maximum δ^{13}C values for each homologue generally occurred at the same depth in P1 with the lowest δ^{13}C values occurring at 3.7 m, with the exception of C_{33} where the lowest δ^{13}C value occurred at 0.2 m. The highest δ^{13}C values in P1 came from 2.8 m for each chain length. In P2, the correlation between minimum and maximum values with depth is not as clear. C_{27} and C_{29} are both ^{13}C-enriched at 6.72 m but have minimum δ^{13}C values at 4.12 m and 2.72 m, respectively. Whereas C_{31} and C_{33} record the most ^{13}C-depleted values at 4.42 m and have maximum δ^{13}C values at 4.72 m and 4.92 m respectively.

3.3. Plant wax *n*-alkanol $\delta^{13}C$

Plant wax δ^{13}C values of *n*-alkanol homologues C_{24}–C_{32} are presented in Tables S5 and S6. The δ^{13}C values of the three dominant homologues C_{26}, C_{28} and C_{30} are presented in Fig. S5. The *n*-alkanol weighted average, which is the mean value for the δ^{13}C values of C_{26}, C_{28} and C_{30} ($\delta^{13}C_{AvgC26\text{-}C30}$), is presented in Fig. 3. Similar to the *n*-alkanes, δ^{13}C values of the *n*-alkanols decrease as the chain length increases in both P1 and P2, with the exception of C_{32}. This is likely due to the low abundance of the compound in the sample (not present in a detectable amount in 12 of 45 samples), as well as possible inaccurate measurement due to its elution close to the C_{33} *n*-alkan-2-one homologue in the GC-MS. The highest and lowest δ^{13}C values do not occur at the same or similar depths in any of the homologues.

3.4. Bulk $\delta^{13}C_{org}$ values

Bulk $\delta^{13}C_{org}$ values fall between −27.4‰ and −22.9‰ in P1 (range of 4.5‰) and exhibit slightly higher values in P2, falling between −26.6‰ and −20.3‰, with an increased range of 6.3‰. These values largely fall within the expected ranges of C_3 photosynthetic vegetation from sedimentary organic matter, which is between approximately −30‰ and −22‰ (Bender, 1971; Farquhar et al., 1989; Vogel, 1978). The bulk $\delta^{13}C_{org}$ values are placed against the *n*-alkane $\delta^{13}C_{AvgC29\text{-}C33}$ and *n*-alkanol $\delta^{13}C_{AvgC26\text{-}C30}$ in Fig. 3. All $\delta^{13}C_{org}$ values are provided in Tables S5 and S6 for P1 and P2, respectively.

4. Discussion

Higher plant biomarkers preserved well in both sediment profiles 1 and 2 of TPL. These biomarkers are believed to reflect the local vegetation surrounding the cave site, which have been deposited in/close to the mouth of the cave and subsequently into the main chamber via aeolian transport and regular slopewash events. Similar *n*-alkyl δ^{13}C values are also observed when depths overlap in both profiles, however these values are not an exact match. Given the 5 m distance between both sediment profiles (see Fig. 1) and subsequent differences in the short-term sedimentation rates between dated layers, sediments from similar depths are not strictly time equivalent. Therefore, short-term climatic events may not be captured in both profiles. Through direct comparisons with modern plant and sediment δ^{13}C data (Garcin et al., 2014; Leider et al., 2013; Liu et al., 2022 *and references therein*; Vogts et al., 2009), we find that δ^{13}C values for both C_{29}–C_{33} *n*-alkanes ranging between −38.0 ± 0.5‰ and −30.7 ± 0.5‰ and C_{26}–C_{30} *n*-alkanols ranging between −38.1 ± 0.5‰ and −29.1 ± 0.3‰ from MIS 5-MIS 1 fall within the expected range of values for C_3 vegetation in tropical/sub-tropical regions (between −37.1‰ and −27.1‰) (Bi et al., 2005; Liu et al., 2022; Vogts et al., 2009) (modern values adjusted to pre-industrial atmospheric CO_2 δ^{13}C of −6.5‰, by adding 1.5‰ (Tipple et al., 2010)).

Visually, there appears to be a correspondence between the *n*-alkane and *n*-alkanol δ^{13}C values (Fig. 3). However, Spearman's rank correlation coefficient testing (as data distributions are non-normal) (Fig. S6) demonstrates that there is only a very weak positive correlation, if not almost no linear relationship ($R = 0.094$, $p = 0.56$). There is also a very weak negative relationship ($R = -0.055$, $p = 0.73$) between the *n*-alkane $\delta^{13}C_{AvgC29\text{-}C33}$ and bulk $\delta^{13}C_{org}$ values (Fig. S7), as well as between the *n*-alkanol $\delta^{13}C_{AvgC26\text{-}C30}$ and the bulk $\delta^{13}C_{org}$ values ($R = -0.11$, $p = 0.51$) (Fig. S8) throughout the sediment sequences. These weak relationships may be due to diagenetic alterations in the sediments as a result of microbial activity. While the *n*-alkanols are likely to be of higher plant origin, as indicated by their CPI values (Tables S3 and S4), they are less resistant to post-depositional reworking than *n*-alkanes (Cranwell, 1981; Meyers and Ishiwatari, 1993) and bulk $\delta^{13}C_{org}$ represents multiple sources of organic material (e.g., microorganisms and anthropogenic materials (Kohn and Cerling, 2002)), which may be the cause of the fluctuations seen in the $\delta^{13}C_{AvgC26\text{-}C30}$ and $\delta^{13}C_{org}$ which are not observed in the $\delta^{13}C_{AvgC29\text{-}C33}$. Therefore, it is likely that it is only the *n*-alkanes that are reflecting changes in vegetation through time in the TPL sediment record.

4.1. Main drivers of the $\delta^{13}C$ *n*-alkane record

δ^{13}C values (C_{27}–C_{33}) fluctuate significantly (9.4‰ in *n*-alkanes) throughout the TPL sediment sequence. For the $\delta^{13}C_{AvgC29\text{-}C33}$ the variation is reduced to 4‰. These large ranges are common in tropical and subtropical regions (Liu et al., 2022). Garcin et al. (2014) observed similar ranges in δ^{13}C values of sedimentary *n*-alkanes from Cameroon, western central Africa which they attributed to be predominantly C_3 vegetation, ranging from −35.5‰ to −24.6‰ (10.9‰).

There are multiple factors that are known to contribute to the δ^{13}C values of *n*-alkanes, which primarily include precipitation, aridity, temperature, altitude and the Canopy Effect (Farquhar et al., 1989; Liu et al., 2022; Medina and Minchin, 1980; van der Merwe and Medina, 1991; Vogel, 1978). As annual temperature variations are minimal in the tropics (e.g., Li and Yang, 2022; Milano et al., 2018), it is highly unlikely that temperature serves as the driving influence. While studies have shown that δ^{13}C values of *n*-alkanes increase with altitude (Körner et al., 1988, 1991; Wu et al., 2017), as TPL is located at the top of Pà Hang Hill at an elevation of 1170 m above sea level, we find it improbable that *n*-alkane δ^{13}C values are predominantly reflecting variations in altitude. The Canopy Effect can significantly influence the δ^{13}C values of *n*-alkanes in forested environments, leading to variations of up to 10‰ between the upper canopy and forest floor (Graham et al., 2014; Medina and Minchin, 1980; van der Merwe and Medina, 1991; Vogel, 1978). However, as vegetation in the upper canopy have shorter lifespans (Reich et al., 1997) and make the greatest contribution to leaf litter biomass (Graham et al., 2014), it is not likely that this is the controlling factor of variations in *n*-alkane δ^{13}C values.

Ultimately, we interpret the variations in the TPL δ^{13}C values of *n*-alkanes to derive from the effect of variations in moisture availability (precipitation) on predominantly C_3 vegetation. During periods of increased moisture availability, δ^{13}C values of C_3 plants are often depleted due to an increase in stomatal conductance and fractionation (Diefendorf et al., 2010; Farquhar et al., 1989). Conversely, during periods of decreased moisture availability, C_3 plants can become water-stressed, leading to a decline in stomatal conductance and plant fractionation levels in attempt to improve its water-use efficiency, resulting in enriched δ^{13}C values (Diefendorf et al., 2010).

Moisture availability in Southeast Asia is predominantly controlled by variations in the strength of the Asian Monsoon (Wang et al., 2005). The Asian Monsoon is characterised by increased rainfall during the Asian summer monsoon (ASM) (May–October) and a decline in rainfall during the winter monsoon (AWM) (November–April) (Wang, 2006). The strength of the ASM is largely driven by thermal differences between the Asian landmass and the Indian and Pacific Oceans, as well as the thermal and dynamic impact of the Tibetan Plateau (Wang et al., 2005). The Western Pacific Warm Pool, Intertropical Convergence Zone (ITCZ),

El Niño Southern Oscillation (ENSO) and Heinrich Events (HE) are also considered additional contributing elements (to varying degrees) to the strength of the monsoons (Lauterbach et al., 2020; Thomson et al., 2021; Wang et al., 2001, 2005).

It has been hypothesised that during periods of climate cooling in the Northern Hemisphere (i.e., MIS 4 and MIS 2), the thermal contrast between the Asian landmass and the Indian and Pacific Oceans is reduced as strong polar easterly winds from the Tibetan Plateau, along with the southward migration of the ITCZ, leads to weakening of the ASM and cooler and drier summer conditions (Wang et al., 2005; Webster et al., 1998). In MIS 4–2, extended periods of reduced moisture may lead to changes in the thickness and extent of closed canopy cover in the surrounding landscape, with a potential rise in areas of woodland and open landscape, as observed during MIS 2 at Tam Hay Marklot, Laos (Bourgon et al., 2020) and at the same latitude at the site of Tham Lod, Thailand (Suraprasit et al., 2021). However, $\delta^{13}C$ values of faunal tooth enamel from Duoi U'Oi, Vietnam also suggest changes in forest composition, with an expansion of montane forests (containing a mixture of deciduous trees and gymnosperms, with shrubs and ferns present in abundance (Zheng and Lei, 1999)) in place of monsoon evergreen forests (primarily characterised by oak trees and shrubs (Zheng and Lei, 1999)) during periods of reduced moisture, as in MIS 4 (Bacon et al., 2018a, 2021). Based on initial observations by Zheng and Lei (1999) who analysed the palynological record of the Leizhou Peninsula, southern China, and located at the same latitudes, Bacon et al. (2021) suggested the landscape of Duoi U'Oi to have experienced an increase in the presence of temperate plants, conifers and ferns in MIS 4.

4.2. Palaeovegetation dynamics at Tam Pà Ling: during and after the presence of H. sapiens

As the error ranges of the interpolated ages of the new TPL chronology from Freidline et al. (2023) are quite large (ranging from ±1882 years to ± 8444 years, Table S1) for each sediment sample, only the broad trends in palaeovegetation and moisture availability through MIS 5 b-MIS 1 are interpreted. Although the two deepest sediment samples (6.92 m and 6.72 m) are outside the current chronology of TPL, similar to TPL7, as these are deposited below the oldest dated sample at 6.67 m, we assume that these samples (Fig. S3) were deposited sometime within MIS 5 and are therefore included in interpretations. During the late stages of MIS 5, *n*-alkane $\delta^{13}C_{AvgC29\text{-}C33}$ values at TPL fall firmly within the ranges expected for C_3 vegetation (Bi et al., 2005; Collister et al., 1994; Liu et al., 2022). This aligns well with the MIS 5 palynological results of Zheng and Lei (1999), which also observed a C_3-dominant landscape.

Low sample density for MIS 5 does not permit the investigation of the considerably drier climate proposed by Milano et al. (2018) at the MIS 5–4 transition. However, the oldest *C. massiei* sample in Milano et al. (2018) was taken from a depth of 4.5 m (initially believed to have been deposited between 78–62 ka). The new chronology by Freidline et al. (2023) now places the deposition of this mollusc to ~54 ka (Table S2), well within MIS 3 (Fig. 4. (c) and (d)). The compiled $\delta^{18}O$ values from Hulu and Sanbao Caves, China (Caballero-Gill et al., 2012; Cheng et al., 2009; Wang et al., 2001, 2008) are presented in Fig. 4(e) for palaeohydrological comparison extending to MIS 5. Variability in the $\delta^{18}O$ values is recorded between ~80 and 70 ka, ultimately declining, representing an increase in rainfall towards the MIS 5–4 transition.

Recent studies by Bacon et al. (2018a, 2021) analysing the $\delta^{13}C$ and $\delta^{18}O$ values of faunal tooth enamel from the nearby caves of Nam Lot and Tam Hang South highlighted a considerable difference in the environmental conditions recorded in each cave. Despite their proximity to one another (~150 m apart at the same elevation of ~1120 m), Tam Hang South returned more depleted $\delta^{18}O$ values compared to Nam Lot during MIS 5. Bacon et al. (2021) considered these results to emphasise the complexity of the local environmental conditions that influence each cave with notable fluctuations of biomes. $\delta^{13}C$ values of the faunal tooth enamel indicate fauna from both sites maintained a predominantly C_3 diet, with the majority feeding in an intermediate rainforest/woodland (Bacon et al., 2021). These findings align well with our *n*-alkane $\delta^{13}C$ values.

While TPL7 was excavated from below the oldest dated sediment, given the undisturbed nature of sediment deposition at the site (Demeter et al., 2015, 2017; Freidline et al., 2023) we propose that this fossil was deposited some time before 77 ± 9 ka, indicating that the first *H. sapiens* present at TPL in late MIS 5 encountered a predominantly C_3 forest environment. While there is no evidence to suggest human occupation and activity in TPL, the fact that *H. sapiens* were present around the site which is 270 km inland from the coast, in a C_3 forested landscape, contributes to the growing body of evidence demonstrating that *H. sapiens* were occupying tropical forests long before the Holocene (Roberts et al., 2015b; Wedage et al., 2019). As put forward by Scerri et al. (2022), research must now consider and actively research tropical forests in the main narrative of human evolution in Southeast Asia and Africa (e.g., Bacon et al., 2023; Shipton et al., 2018).

Moving into MIS 4, *n*-alkane $\delta^{13}C_{AvgC29\text{-}C33}$ values range between −36.5 ± 0.6‰ and −34.1 ± 1.5‰ (Fig. 4 (b)). Minor fluctuations (±2.4‰) of the *n*-alkane $\delta^{13}C$ values indicate that moisture availability was locally largely stable throughout MIS 4 with C_3 forests prevailing. Although the *H. sapiens'* remains from TPL are not directly dated, the sediments from which they were excavated reveal that both TPL6 and TPL4 were deposited in similar palaeoenvironmental conditions (Fig. 4 (b)) characterised by relatively consistent moisture availability. The *n*-alkane $\delta^{13}C$ values demonstrate that humans present around TPL during MIS 4 would have existed in and travelled through a heavily forested landscape.

Relatively high and consistent moisture availability appears to contrast the findings of Wang et al. (2008) who observed a decline in ASM intensity during MIS 4 and a subsequent rise in drier conditions, reflected by an increase in the speleothem $\delta^{18}O$ values at Hulu Cave. However, elsewhere in China Zheng and Lei (1999) recorded a shift in the forest composition from tropical evergreen rainforest (consisting of dipterocarps in the upper canopy, with small bushes, shrubs and wild grasses in the lower canopy) which prevail in warmer and wetter climatic conditions such as those in MIS 5, to temperate forests, characterised by a rise in conifers, shrubs, herbs and ferns, and associated with cooler and drier climates in MIS 4, likely in response to the decline in moisture availability. Bacon et al. (2018a, 2021) also found the $\delta^{13}C$ and $\delta^{18}O$ values of faunal tooth enamel from Duoi U'Oi, Vietnam to indicate a transformation in forest composition, potentially from monsoon evergreen forests to montane forests, based on results from Zheng and Lei (1999). Therefore, it is possible that while C_3 forest vegetation prevailed during MIS 4 at TPL, the composition of the forest vegetation may have undergone similar changes to those observed in China (Zheng and Lei, 1999) and Vietnam (Bacon et al., 2018a, 2021). Additional palaeovegetation proxy analysis (e.g., pollen and sedaDNA) to investigate this further is recommended.

MIS 3 is recorded in both P1 and P2, with the $\delta^{13}C_{AvgC29\text{-}C33}$ values varying by 3.9‰ and correlating well overall at similar depths in the two profiles (Fig. 4 (a) and (b)). This range in $\delta^{13}C_{AvgC29\text{-}C33}$ values indicate a rise in the seasonal variability of moisture availability during this period. When compared to the $\delta^{18}O$ and $\delta^{13}C$ values of the *C. massiei* from Milano et al. (2018) now placed against the revised chronology (Fig. 4(c) and (d)), similar fluctuations are observed. This indicates that variations in moisture availability led to water-stressed conditions for C_3 vegetation (Farquhar et al., 1989), resulting in potential changes in the surrounding C_3 landscape (i.e., breaks in the forest canopy, with a potential increase in open patches of shrubs/grasses). While multiple stadials, interstadials and HEs are known to have occurred during MIS 3 (e.g., Lauterbach et al., 2020), these occurred over short periods which our current sample and age resolution cannot account for.

Although MIS 3 was characterised by fluctuations in moisture availability leading to variations in C_3 vegetation dynamics, the three

H. sapiens known to have been present at the site towards the beginning (TPL1, 2 & 5) (Fig. 4(a)) and the end (TPL3) of MIS 3 (Fig. 4(b)), would have all encountered a predominantly wet and forested C_3 environment. This corroborates Bourgon et al. (2021) who found the $\delta^{13}C$ values (−26.4‰) of two teeth from the *H. sapiens* individual TPL1 to demonstrate that they obtained their food from a C_3 forested environment and the more recent study by Bacon et al. (2023) who found *Homo* sp. at Duoi U'Oi would have relied on rainforests from ~70 ka. *H. sapiens* present during MIS 3 (~46 ka) would have been dependent on forest resources and the utilisation of diverse hunting techniques (Bacon et al., 2023).

MIS 2 is more condensed in the sediment record, with only 8 samples (4 from both P1 and P2). *n*-alkane $\delta^{13}C_{AvgC29\text{-}C33}$ values remain relatively consistent at ~ -34.5‰ in P1 (ranging by 0.5‰), whereas P2 values vary by 3.7‰. This is a potential reflection of the differences in sedimentation rates between both profiles. During MIS 2, the surrounding ecosystem of TPL likely consisted of a forest-grassland mosaic landscape similar to Tham Lod (Marwick and Gagan, 2011; Suraprasit et al., 2021) at the same latitude. These sites, along with that of Boh Dambang, located farther south in Cambodia (Bacon et al., 2018b), suggest that C_3 forested vegetation remained the dominating plant type on MSEA. A prevailing C_3 landscape during MIS 2 was also observed in Hang Trông, Vietnam (Rabett et al., 2017), Tam Hay Marklot, Laos (Bourgon et al., 2020) and Nong Pa Kho, northeastern Thailand (Penny, 2001). Similar to Suraprasit et al. (2021), not all climatic events known to have occurred in MIS 2 (i.e., the Bølling-Allerød and the Younger Dryas) are distinguishable in this palaeoenvironmental record. For a more robust interpretation of MIS 2, more sediment samples at shorter increments for further biomarker analysis are recommended, ideally in tandem with additional proxy applications (i.e., pollen analysis).

Seven sediment samples from 1.4 m and above in P1 represent MIS 1 (i.e., the Holocene). $\delta^{13}C_{AvgC29\text{-}C31}$ values are relatively stable at ~34.5‰. We believe this to be the result of predominantly consistent moisture availability during the Holocene. This period saw the rise of sea levels to their current levels, an increase in the land-ocean thermal gradient and the strengthening of the ASM, with the palaeoenvironmental records from Hulu, Sanbao and Dongge Caves (Cheng et al., 2009; Dykoski et al., 2005; Wang et al., 2001, 2008), Tham Lod (Marwick and Gagan, 2011) and Hang Trông (Rabett et al., 2017) all recording an apparent increase in moisture availability. Overall, much like observations by Milano et al. (2018), $\delta^{13}C$ *n*-alkane values indicate that the landscape of TPL was characterised by C_3 forest vegetation, likely looking similar to how it is today.

5. Conclusions

Analysis of higher plant biomarkers from TPL suggests that the surrounding landscape consisted of predominantly C_3 vegetation throughout MIS 5 b-MIS 1. The *n*-alkane $\delta^{13}C$ values are interpreted as reflecting this dominance. The $\delta^{13}C$ values of *n*-alkanols and bulk organic carbon were determined to have been subject to post-depositional modifications (likely as a result of microbial reworking) and were therefore excluded from palaeovegetation interpretations. While the landscape of TPL was comprised of C_3 forest vegetation from the late stages of MIS 5 and through MIS 4, when compared with the existing palaeoenvironmental records (e.g., pollen and fauna proxies) for MIS 5–4 of Zheng and Lei (1999) and Bacon et al. (2018a, 2021), it is possible that the C_3 vegetation dynamics underwent significant changes (i.e., an increase in temperate forest in place of rainforest at the MIS 5–4 transition). Significant *n*-alkane $\delta^{13}C$ fluctuations in MIS 3 were inferred to reflect inconsistent moisture availability, with consequences for C_3 vegetation dynamics around TPL, potentially leading to the expansion of patches of open landscape (e.g., shrubs and/or some grasses). Our data suggests C_3 vegetation prevailed throughout MIS 2 and MIS 1.

Our palaeovegetation reconstruction suggests that the first known *H. sapiens* to be present in and around the site during MIS 5, 4 and 3 were existing in potentially dense C_3 forest vegetation during periods of moderate moisture availability and were not restricted to areas of open landscape or traversing these inland locations strictly during drier conditions. Future studies should seek to apply different proxies (e.g., sedaDNA and *n*-alkane δD) to improve the palaeoenvironmental (both palaoevegetation and palaeohydrology) reconstruction of TPL. An increased sample resolution for each MIS and a collection of modern sediment and vegetation samples for modern calibrations is also advised to develop a more refined palaeoenvironmental reconstruction.

Credit author statement

Conceptualisation: M.S.M-H, A.J.B, F.A.M and M.W.M, Formal analysis: M.S.M-H, A.J.B, F.A.M, A.I.H, K.G, Writing – original draft: M. S.M-H, Writing – review & editing: A.J.B, F.A.M, M.W.M, A.I.H, K.G, J.J. T, T.D, K.E.W, R.J-B. S.B, N.B, T.E.D, S.F, T.L, P.S, V.S, E.S, A.Z, C.Z, A-M.B, P.D, J-J.H, L.S & F.D

Declaration of competing interest

The authors declare that they have no known competing financial interests or personal relationships that could have appeared to influence the work reported in this paper.

Data availability

Data will be made available on request.

Acknowledgements

M.S.M-H would like to thank Peter Hopper for his GC-MS and ChemStation support at WA-OIGC, Curtin University. M.S.M-H would also like to thank Dr. Helena Andersson and Dr. Russell Fuller from Flinders Analytical, Flinders University for the use of the EA-IRMS and providing the bulk $\delta^{13}C$ values of TPL sediment samples.

M.S.M-H undertook this research supported by Flinders University College of Humanities, Arts and Social Sciences through a Future Fellowship Postgraduate Scholarship.

M.W.M thanks the Australian Research Council for ongoing support with a Future Fellowship (FT180100309).

Appendix A. Supplementary data

Supplementary data to this article can be found online at https://doi.org/10.1016/j.quascirev.2023.108471.

References

Bacon, A.-M., Bourgon, N., Dufour, E., Demeter, F., Zanolli, C., Westaway, K.E., Joannes-Boyau, R., Duringer, P., Ponche, J.-L., Morley, M.M., Suzzoni, E., Frangeul, S., Boesch, Q., Antoine, P.O., Boualaphane, S., Sichanthongtip, P., Sihanam, D., Huong, N.T.M., Tuan, N.A., Fiorillo, D., Tombret, O., Patole-Edoumba, E., Zachwieja, A., Luangkhoth, T., Souksavatdy, V., Dunn, T.E., Shackelford, L.L., Hublin, J.J., 2023. Palaeoenvironments and dynamics of hominin evolution in Southeast Asia. Sci. Rep. 13, 16165 https://doi.org/10.1038/s41598-023-43011-2.

Bacon, A.-M., Bourgon, N., Dufour, E., Zanolli, C., Duringer, P., Ponch, J.-L., Antoine, P.-O., Shackelford, L., Huong, N.T.M., Sayavonkhamdy, T., Patole-Edoumba, E., Demeter, F., 2018a. Nam Lot (MIS 5) and Duoi U'oi (MIS 4) southeast asian sites revisited: zooarchaeological and isotopic evidences. Palaeogeogr. Palaeoclimatol. Palaeoecol. 512, 132–144. https://doi.org/10.1016/j.palaeo.2018.03.034.

Bacon, A.-M., Bourgon, N., Welker, F., Cappellini, E., Fiorillo, D., Tombret, O., Huong, N. T.M., Tuan, N.A., Sayavonkhamdy, T., Souksavatdy, V., Sichanthongtip, P., Antoine, P.-O., Duringer, P., Ponche, J.-L., Westway, K.E., Joannes-Boyau, R., Boesch, Q., Suzzoni, E., Frangeul, S., Patole-Edoumba, E., Zachwieja, A., Shackelford, L., Demeter, F., Hublin, J.-J., Dufour, E., 2021. A multi-proxy approach to exploring *Homo sapiens'* arrival, environments and adaptions in Southeast Asia. Sci. Rep. 11, 21080 https://doi.org/10.1038/s41598-021-99931-4.

Bacon, A.-M., Duringer, P., Westaway, K., Joannes-Boyau, R., Zhao, J-x., Bourgon, N., Dufour, E., Pheng, S., Tep, S., Ponche, J.-L., Barnes, L., Blin, A., Patole-Edoumba, E., Demeter, F., 2018b. Testing the savannah corridor hypothesis during MIS2: the Boh

Dambang hyena site in southern Cambodia. Quat. Int. 464 (Part B), 417–439. https://doi.org/10.1016/j.quaint.2017.10.047.
Bae, C.J., Douka, K., Petraglia, M.D., 2017. On the origins of modern humans: Asian perspectives. Science 358, 1269. https://doi.org/10.1126/science.aai9067.
Bender, M.M., 1971. Variations in the $^{13}C/^{12}C$ ratios of plants in relation to the pathway of photosynthetic carbon dioxide formation. Phytochemistry 10 (6), 1239–1244. https://doi.org/10.1016/S0031-9422(00)84324-1.
Bettis, E.A., Milius, A.K., Carpenter, S.J., Larick, R., Zaim, Y., Rizal, Y., Ciochon, R.L., Tassier-Surine, S.A., Murray, D., Suminto, Bronto, S., 2009. Way out of Africa: early Pleistocene paleoenvironments inhabited by *Homo erectus* in sangiran, java. J. Hum. Evol. 56 (1), 11–24. https://doi.org/10.1016/j.jhevol.2008.09.003.
Bi, X., Sheng, G., Liu, X., Li, C., Fu, J., 2005. Molecular and carbon and hydrogen isotopic composition of n-alkanes in plant leaf waxes. Org. Geochem. 36 (10), 1405–1417. https://doi.org/10.1016/j.orggeochem.2005.06.001.
Bird, M.I., Taylor, D., Hunt, C., 2005. Palaeoenvironments of insular Southeast Asia during the last glacial period: a savanna corridor in sundaland? Quat. Sci. Rev. 24 (20–21), 2228–2242. https://doi.org/10.1016/j.quascirev.2005.04.004.
Boivin, N., Fuller, D.Q., Dennell, R., Allaby, R., Petraglia, M., 2013. Human dispersal across diverse environments of Asia during the upper Pleistocene. Quat. Int. 300, 32–47. https://doi.org/10.1016/j.quaint.2013.01.008.
Bourgon, N., Jaouen, K., Bacon, A.-M., Dufour, E., McCormack, J., Han Tran, N.-., Trost, M., Fiorillo, D., Dunn, T.E., Zanolli, C., Zachwieja, A., Duringer, P., Ponche, J.-L., Boesch, Q., Antoine, P.-O., Westaway, K.E., Joannes-Boyau, R., Suzzoni, E., Frangeul, S., Crozier, F., Aubaile, F., Patole-Edoumba, E., Luangkhoth, T., Souksavatdy, V., Boualaphane, S., Sayavonkhamdy, T., Sichanthongtip, P., Sihanam, D., Demeter, F., Shackelford, L.L., Hublin, J.-J., Tütken, T., 2021. Trophic ecology of a Late Pleistocene early modern human from tropical Southeast Asia inferred from zinc isotopes. J. Hum. Evol. 161, 103075 https://doi.org/10.1016/j.jhevol.2021.103075.
Bourgon, N., Jaouen, K., Bacon, A.-M., Jochum, K.P., Dufour, E., Duringer, P., Ponche, J.-L., Joannes-Boyau, R., Boesch, Q., Antoine, P.-O., Hullot, M., Weis, U., Schulz-Kornas, E., Trost, M., Fiorillo, D., Demeter, F., Patole-Edoumba, E., Shackelford, L., Dunn, T.E., Zachwieja, A., Duangthongchit, S., Sayavonkhamdy, T., Sichanthongtip, P., Sihanam, D., Souksavatdy, V., Hublin, J.-J., Tütken, 2020. Zinc isotopes in Late Pleistocene fossil teeth from a Southeast Asian cave setting preserve paleodietary information. Proc. Natl. Acad. Sci. USA 117 (9), 4675–4681. https://doi.org/10.1073/pnas.1911744117.
Bradshaw, C.J.A., Norman, K., Ulm, S., Williams, A.N., Clarkson, C., Chadœuf, J., Lin, S. C., Jacobs, Z., Roberts, R.G., Bird, M.I., Weyrich, L.S., Haberle, S.G., O'Connor, S., Llamas, B., Cohen, T.J., Friedrich, T., Veth, P., Leavesley, M., Saltré, F., 2021. Stochastic models support rapid peopling of Late Pleistocene Sahul. Nat. Commun. 12 (2240) https://doi.org/10.1038/s41467-021-21551-3.
Bray, E.E., Evans, E.D., 1961. Distribution of *n*-paraffins as a clue to recognition of source beds. Geochem. Cosmochim. Acta 22 (1), 2–15. https://doi.org/10.1016/0016-7037(61)90069-2.
Caballero-Gill, R.P., Clemens, S.C., Prell, W.L., 2012. Direct correlation of Chinese speleothem $\delta^{18}O$ and South China Sea planktonic $\delta^{18}O$: transferring a speleothem chronology to the benthic marine chronology. Paleoceanogr. Paleoclimatol. 27 (2) https://doi.org/10.1029/2011PA002268.
Cheng, H., Edwards, R.L., Broecker, W.S., Denton, G.H., Kong, X., Wang, Y., Zhang, R., Wang, X., 2009. Ice age terminations. Science 326 (5950), 248–252. https://doi.org/10.1126/science.1177840.
Chiang, J.C.H., Kong, W., Wu, C.H., Battisti, D.S., 2020. Origins of East Asian summer monsoon seasonality. J. Clim. 33, 7945–7965. https://doi.org/10.1175/JCLI-D-19-0888.1.
Chikaraishi, Y., Naraoka, H., 2007. δ13C and δD relationships among three n-alkyl compound classes (n-alkanoic acid, n-alkane and n-alkanol) of terrestrial higher plants. Org. Geochem. 38 (2), 198–215. https://doi.org/10.1016/j.orggeochem.2006.10.003.
Collister, J.W., Rieley, G., Stern, B., Eglinton, G., Fry, B., 1994. Compound-specific $\delta^{13}C$ analyses of leaf lipids from plants with differing carbon dioxide metabolisms. Org. Geochem. 21 (6–7), 619–627. https://doi.org/10.1016/0146-6380(94)90008-6.
Cranwell, P.A., 1981. Diagenesis of free and bound lipids in terrestrial detritus deposited in a lacustrine sediment. Org. Geochem. 3 (3), 79–89. https://doi.org/10.1016/0146-6380(81)90002-4.
Demeter, F., Shackleford, L.L., Bacon, A.-M., Duringer, P., Westaway, K., Sayavongkhamdy, T., Braga, J., Sichanthongtip, P., Khamdalavong, P., Ponche, J.-L., Wang, H., Lundstorm, C., Patole-Edoumba, E., Karpoff, A.-M., 2012. Anatomically modern human in Southeast Asia (Laos) by 46 ka. Proc. Natl. Acad. Sci. USA 109 (36), 14375–14380. https://doi.org/10.1073/pnas.1208104109.
Demeter, F., Shackleford, L.L., Westaway, K., Barnes, L., Duringer, P., Ponche, J.-L., Dumoncel, J., Sénégas, F., Sayavongkharndy, T., Zhao, J.-X., Sichanthongtip, P., Patole-Edoumba, E., Dunn, T., Zachwieja, A., Coppens, Y., Willerslev, E., Bacon, A.-M., 2017. Early modern humans from Tam Pà ling, Laos. Curr. Anthropol. 58 (17), S527–S537.
Demeter, F., Shackleford, L., Westaway, K., Duringer, P., Bacon, A.-M., Ponche, J.-L., Wu, X., Sayavongkharndy, T., Zhao, J.-X., Barnes, L., Boyon, M., Sichanthongtip, P., Sénégas, F., Karpoff, A.-M., Patole-Edoumba, E., Coppens, Y., Braga, J., 2015. Early modern humans and morphological variation in Southeast Asia: fossil evidence from Tam Pà ling, Laos. PLoS One 10 (4), e0121193. https://doi.org/10.1371/journal.pone.0121193.
Demeter, F., Zanolli, C., Westaway, K.E., Joannes-Boyau, R., Duringer, P., Morley, M.W., Welker, F., Rüther, P.L., Skinner, M.M., McColl, H., Gaunitz, C., Vinner, L., Dunn, T. E., Olsen, J.V., Sikora, M., Ponche, J.-L., Suzzoni, E., Frangeul, S., Boesch, Q., Antoine, P.O., Pan, L., Xing, S., Zhao, J.-X., Bailey, R.M., Boualaphane, S., Sichanthongtip, P., Sihanam, D., Patole-Edoumba, E., Aubaile, F., Crozier, F., Bourgon, N., Zachwieja, A., Luangkhoth, T., Souksavatdy, V., Sayavongkhamdy, T., Cappellini, E., Bacon, A.-M., Hublin, J.J., Willerslev, E., Shackelford, L., 2022. A Middle Pleistocene denisovan from the annamite chain of northern Laos. Nat. Commun. 13 (2557) https://doi.org/10.1038/s41467-022-29923-z.
Diefendorf, A.F., Freeman, K.H., Wing, S.L., Graham, H.V., 2011. Production of *n*-alkyl lipids in living plants and implications for the geological past. Geochem. Cosmochim. Acta 75 (23), 7472–7485. https://doi.org/10.1016/j.gca.2011.09.028.
Diefendorf, A.F., Freimuth, E.J., 2017. Extracting the most from terrestrial plant-derived n-alkyl lipids and the carbon isotopes from the sedimentary record. Org. Geochem. 103, 1–21. https://doi.org/10.1016/j.orggeochem.2016.10.016.
Diefendorf, A.F., Mueller, K.E., Wing, S.L., Koch, P.L., Freeman, K.H., 2010. Global patterns in leaf ^{13}C discrimination and implications for studies of past and future climate. Proc. Natl. Acad. Sci. USA 107 (13), 5738–5743. https://doi.org/10.1073/pnas.0910513107.
Duringer, P., Bacon, A.-M., Sayavongkhamdy, T., Nguyen, T.K.T., 2012. Karst development, breccias history, and mammalian assemblages in Southeast Asia: a brief review Karst development, breccia history, and mammalian assemblagesof Southeast Asia. Palevol Reports 11 (2–3), 133–157. https://doi.org/10.1016/j.crpv.2011.07.003.
Dykoski, C.A., Edwards, R.L., Cheng, H., Yuan, D., Cai, Y., Zhang, M., Lin, Y., Qing, J., An, Z., Revenaugh, J., 2005. A high-resolution, absolute-dated Holocene and deglacial Asian monsoon record from Dongge Cave, China. Earth Planet Sci. Lett. 233 (1–2), 71–86. https://doi.org/10.1016/j.epsl.2005.01.036.
Edwards, E.J., 2019. Evolutionary trajectories, accessibility and other metaphors: the case of C_4 and CAM photosynthesis. New Phytol. 223 (4), 1742–1755. https://doi.org/10.1111/nph.15851.
Eglinton, G., Gonzalez, A.G., Hamilton, R.J., Raphael, R.A., 1962. Hydrocarbon constituents of the wax coatings of plant leaves: a taxonomic survey. Phytochemistry 1 (2), 89–102. https://doi.org/10.1016/S0031-9422(00)88006-1.
Eglinton, G., Hamilton, R.J., 1967. Leaf Epicuticular Waxes: the waxy outer surfaces of most plants display a wide diversity of fine structure and chemical constituents. Science 156 (3780), 1322–1335. https://doi.org/10.1126/science.156.3780.1322.
Eiserbeck, C., Nelson, R.K., Grice, K., Curiale, J., Reddy, C.M., 2012. Comparison of GC-MS, GC-MRM-MS, and GCxGC to characterise higher plant biomarkers in Tertiary oils and rock extracts. Geochem. Cosmochim. Acta 87, 299–322. https://doi.org/10.1016/j.gca.2012.03.033.
Farquhar, G.D., Ehleringer, J.R., Hubick, K.T., 1989. Carbon isotope discrimination and photosynthesis. Annu. Rev. Plant Physiol. Plant Mol. Biol. 40, 503–537.
Freidline, S.E., Westaway, K.E., Joannes-Boyau, R., Duringer, P., Ponche, J.-L., Morley, M.W., Hernandez, V.C., McAllister-Hayward, M.S., McColl, H., Zanolli, C., Gunz, P., Bergmann, I., Sichanthongtip, P., Sihanam, D., Boulaphane, S., Luangkhoth, T., Souksavatdy, V., Dosseto, A., Demeter, F., 2023. Early presence of *Homo sapiens* in Southeast Asia by 86-68 kyr at Tam Pà ling, northern Laos. Nat. Commun. 14 (3193) https://doi.org/10.1038/s41467-023-38715-y.
Fromaget, J., 1936. Sur la stratigraphie des formations récentes de la Chaîne annamitique septentrionale et sur l'existence de l'Homme dans le Quaternarie inférieur de cette partie de l'Indochine. C. R. Acad. Sci. Paris 203, 738–741.
Fromaget, J., 1937. *Aperçu sur la Stratigraphie et l'Anthropologie préhistorique des formations récentesdans la Chaîne Annamitique et le Haut-Laos*. Compte rendu de la douzième session du Congrès préhistorique de France, pp. 785–798. Toulous-Foix.
Fromaget, J., 1940. Les récentes découvertes anthropologiques dans les formations préhistoriques de la chaîne annamitique. Government Printer, Singapore, pp. 51–59.
Gamble, C.S., 1993. Timewalkers: the Prehistory of Global Colonization. Alan Sutton Press, Stroud.
Gamble, C.S., 2013. Settling the Earth: the Archaeology of Deep Human History. Cambridge University Press, Cambridge.
Garcin, Y., Schefuß, E., Schwab, V.F., Garreta, V., Gleixner, G., Vincens, A., Todou, G., Séné, O., Onana, J.-M., Achoundong, G., Sachse, D., 2014. Reconstructing C_3 and C_4 vegetation cover using n-alkane carbon isotope ratios in recent lake sediments from Cameroon, Western Central Africa. Geochem. Cosmochim. Acta 142, 482–500. https://doi.org/10.1016/j.gca.2014.07.004.
Graham, H.V., Patzkowsky, M.E., Wing, S.L., Parker, G.G., Fogel, M.L., Freeman, K.H., 2014. Isotopic characteristics of canopies in simulated leaf assemblages. Geochem. Cosmochim. Acta 144, 82–95. https://doi.org/10.1016/j.gca.2014.08.032, 10.1016/j.gca.2014.08.032.
Grimalt, J.O., Torras, E., Albaigés, J., 1988. Bacterial reworking of sedimentary lipids during sample storage. Org. Geochem. 13 (4–6), 741–746. https://doi.org/10.1016/0146-6380(88)90096-4.
Joordens, J.C.A., d'Errico, F., Wesselingh, F.P., Munro, S., de Vos, J., Wallinga, J., Ankjærgaard, C., Reimann, T., Wijbrans, J.R., Kuiper, K.F., Mücher, H.J., Coqueugniot, H., Prié, V., Joosten, I., van Os, B., Schulp, A.S., Panuel, M., van der Haas, V., Lustenhouwer, W., Reijmer, J.J.G., Roebroeks, W., 2016. Homo erectus at Trinil on Java used shells for tool production and engraving. Nature 518, 228–231. https://doi.org/10.1038/nature13962.
Jetter, R., Kunst, L., Samuels, A.L., 2006. Composition of plant cuticular waxes. In: Riederer, M., Müller, C. (Eds.), Biology of the Plant Cuticle. Blackwell, Oxford.
Kohn, M.J., Cerling, T.E., 2002. Stable isotope compositions of biological apatite. Rev. Mineral. Geochem. 48 (1), 455–488. https://doi.org/10.2138/rmg.2002.48.12.
Körner, Ch, Farquhar, G.D., Roksandic, Z., 1988. A global survey of carbon isotope discrimination in plants from high altitude. Oecologia 74, 623–632. https://doi.org/10.1007/BF00380063.
Körner, Ch, Farquhar, G.D., Wong, S.C., 1991. Carbon isotope discrimination by plants follow latitudinal and altitudinal trends. Oecologia 88, 30–40. https://doi.org/10.1007/BF00328400.
Langley, M.C., Clarkson, C., Ulm, S., 2008. Behavioural complexity in eurasian neanderthal populations: a chronological examination of the archaeological

evidence. Camb. Archaeol. J. 18 (3), 289–307. https://doi.org/10.1017/S0959774308000371.
Lauterbach, S., Andersen, N., Wang, Y.V., Blanz, T., Larsen, T., Schneider, R.R., 2020. An ~130 kyr record of surface water temperature and $\delta^{18}O$ from the northern bay of bengal: investigating the linkage between Heinrich events and weak monsoon intervals in Asia. Paleoceanogr. Paleoclimatol. 35 (2) https://doi.org/10.1029/2019PA003646.
Leider, A., Hinrichs, K.-U., Schefuß, E., Versteegh, G.J.M., 2013. Distribution and stable isotopes of plant wax derived n-alkanes in lacustrine, fluvial and marine surface sediments along an Eastern Italian transect and their potential to reconstruct the hydrological cycle. Geochem. Cosmochim. Acta 117, 16–32. https://doi.org/10.1016/j.gca.2013.04.018.
Li, P., Yang, Y., 2022. Swidden agriculture landscape mapping using MODIS vegetation index time series and its spatio-temporal dynamics in northern Laos. Rem. Sens. 14 (23), 6173. https://doi.org/10.3390/rs14236173.
Liu, J., An, Z., 2020. Leaf wax n-alkane carbon isotope values vary among major terrestrial plant groups: different responses to precipitation amount and temperature, and implications of palaeoenvironmental reconstruction. Earth Sci. Rev. 202, 103081 https://doi.org/10.1016/j.earscirev.2020.103081.
Liu, J., Zhao, J., He, D., Huang, X., Jiang, C., Yan, H., Lin, G., An, Z., 2022. Effects of plant types on terrestrial leaf wax long-chain *n*-alkane biomarkers: implications and palaeoapplications. Earth Sci. Rev. 235, 104248 https://doi.org/10.1016/j.earscirev.2022.104248.
Lloyd, J., Farquhar, G.D., 1994. ^{13}C discrimination during CO_2 assimilation by the terrestrial biosphere. Oecologia 99, 201–215. https://doi.org/10.1007/BF00627732.
Logan, G.A., Boon, J.J., Eglinton, G., 1993. Structural biopolymer preservation in Miocene leaf fossils from the Clarkia site, northern Idaho. Proc. Natl. Acad. Sci. USA 90 (6), 2246–2250. https://doi.org/10.1073/pnas.90.6.2246.
Louys, J., Duval, M., Price, G.J., Westaway, K., Zaim, Y., Rizal, Y., Aswan, Puspaningrum, M., Trihascaryo, A., Breitenbach, S.F.M., Kwiecien, O., Cai, Y., Higgins, P., Albers, P.C.H., de Vos, J., Roberts, P., 2022. Speleological and Environmental History of Lida Ajer Cave, Western Sumatra, vol. 377. Philosophical Transactions of the Royal Society B. https://doi.org/10.1098/rstb.2020.0494, 1849.
Louys, J., Roberts, P., 2020. Environmental drivers of megafauna and hominin extinction in Southeast Asia. Nature 586, 402–406. https://doi.org/10.1038/s41586-020-2810-y.
Marwick, B., Gagan, M.K., 2011. Late Pleistocene monsoon variability in northwest Thailand: an oxygen isotope sequence from the bivalve Margaritanopsis laosensis excavated in Mae Hong Son province. Quat. Sci. Rev. 30, 3088–3098. https://doi.org/10.1016/j.quascirev.2011.07.007.
Marzi, R., Torkelson, B.E., Oslon, R.K., 1993. A revised carbon preference index. Organic Geochemistry 20 (8), 1303–1306. https://doi.org/10.1016/0146-6380(93)90016-5.
McAllister, M.S., Morley, M.W., Tyler, J.J., McInerney, F.A., Blyth, A.J., 2022. Investigating the palaeoenvironmental context of Late Pleistocene human dispersals into Southeast Asia: a review of stable isotope applications. Archaeol. Anthropol. Sci. 14 (86) https://doi.org/10.1007/s12520-022-01540-3.
Medina, E., Minchin, P., 1980. Stratification of $\delta^{13}C$ values of leaves in Amazonian rain forests. Oecologia 45, 377–378. https://doi.org/10.1007/BF00540209.
Meyers, P.A., Ishiwatari, R., 1993. Lacustrine organic geochemistry – an overview of indicators of organic matter sources and diagenesis in lake sediments. Org. Geochem. 20 (7), 867–900. https://doi.org/10.1016/0146-6380(93)90100-P.
Milano, S., Demeter, F., Hublin, J.-J., Duringer, P., Patole-Edoumba, E., Ponche, J.-L., Shackelford, L., Boesch, Q., Houng, N.T.M., Lan, L.T.P., Duangthongchit, S., Sayavonkhamdy, T., Sichanthongtip, P., Sihanam, D., Souksavatdy, T., Westaway, K., Bacon, A.-M., 2018. Environmental conditions framing the first evidence of modern humans at Tam Pà Ling, Laos: a stable isotope record from terrestrial gastropod carbonates. Palaeogeogr. Palaeoclimatol. Palaeoecol. 511, 352–363. https://doi.org/10.1016/j.palaeo.2018.08.020.
Nguyen, T.T.T., Egasse, C., Anquetil, C., Zanetti, F., Zeller, B., Huon, S., Derenne, S., 2017. Leaf lipid degradation in soils and surface sediments: a litterbag experiment. Org. Geochem. 104, 35–41. https://doi.org/10.1016/j.orggeochem.2016.12.001.
Nie, Y., Chi, C.-Q., Fang, H., Liang, J.-L., Lu, S.-L., Lai, G.-L., Tang, Y.-Q., Wu, X.-L., 2014. Diverse alkane hydroxylase genes in microorganisms and environments. Sci. Rep. 4, 4968. https://doi.org/10.1038/srep04968.
O'Connell, J.F., Allen, J., Williams, M.A.J., Williams, A.N., Turney, C.S.M., Spooner, N. A., Kamminga, J., Brown, G., Cooper, A., 2018. When did *Homo sapiens* first reach Southeast Asia and sahul? Proc. Natl. Acad. Sci. USA 115 (34), 8482–8490. https://doi.org/10.1073/pnas.1808385115.
Patalano, R., Arthur, C., Carleton, W.C., Challis, S., Dewar, G., Gayantha, K., Gleixner, G., Ilgner, J., Lucas, M., Marzo, S., Mokhachane, R., Pazan, K., Spurite, D., Morley, M. W., Parker, A., Mitchell, P., Stewart, B.A., Roberts, P., 2023. Ecological stability of Late Pleistocene-to-Holocene Lethoso, southern Africa, facilitated human upland habitation. Commun. Earth & Environ. 4 (129) https://doi.org/10.1038/s43247-023-00784-8.
Patalano, R., Roberts, P., Boivin, N., Petraglia, M.D., Mercader, J., 2021. Plant wax biomarkers in human evolutionary studies. Evol. Anthropol. Issues News Rev. https://doi.org/10.1002/evan.21921.
Penny, D., 2001. A 40,000 year palynological record from north-east Thailand; implications for biogeography and palaeo-environmental reconstruction. Palaeogeogr. Palaeoclimatol. Palaeoecol. 171 (3–4), 97–128. https://doi.org/10.1016/S0031-0182(01)00242-5.
Rabett, R., Ludgate, N., Stimpson, C., Hill, E., Hunt, C., Ceron, J., Farr, L., Morley, M., Reynolds, T., Zukswert, H., Simpson, D., Nyiri, B., Verhoeven, M., Appleby, J., Meneely, J., Phan, L., Dong, N.-N., Llyod-Smith, L., Hawkes, J., Blyth, A.J., Nguyen, C.T., 2017. Tropical limestone resilience and late Pleistocene foraging during MIS-2 in the Tràng An, Massif. Quat. Int. 448, 62–81. https://doi.org/10.1016/j.quaint.2016.06.010.
Reich, P.B., Walters, M.B., Ellsworth, D.S., 1997. From tropics to tundra: global convergence in plant functioning. Proc. Natl. Acad. Sci. USA 94 (25), 13730–13734. https://doi.org/10.1073/pnas.94.25.13730.
Reyes-Centeno, H., 2016. Out of Africa and into Asia: fossil and genetic evidence on modern human origins and dispersals. Quat. Int. 416, 249–262. https://doi.org/10.1016/j.quaint.2015.11.063.
Rieley, G., 1994. Derivatization of organic compounds prior to gas chromatographic-combustion-isotope ratio mass spectrometric analysis: identification of isotope fractionation processes. Analyst 119, 915–919. https://doi.org/10.1039/AN9941900915.
Rizal, Y., Westaway, K.E., Zaim, Y., van den Bergh, G.D., Bettis III, E.A., Morwood, M.J., Huffman, O.F., Grün, R., Joannes-Boyau, R., Bailey, R.M., Sidarto, Westaway, M.C., Kurniawan, I., Moore, M.W., Storey, M., Aziz, F., Suminto, Zhao, J-x., Aswan, Sipola, M.E., Larick, R., Zonneveld, J.-P., Scott, R., Putt, S., Ciochon, R.L., 2020. Last appearance of *Homo erectus* at ngandong, java, 117,000-108,000 years ago. Nature 577, 381–385. https://doi.org/10.1038/s41586-019-1863-2.
Roberts, P., Boivin, N., Petraglia, M., 2015a. The Sri Lankan 'microlithic' tradition c. 38,000 to 3,000 Years ago: tropical technologies and adaptations of *Homo sapiens* at the southern edge of Asia. J. World PreHistory 28, 69–112. https://doi.org/10.1007/s10963-015-9085-5.
Roberts, P., Perera, N., Wedage, O., Deraniyagala, S., Perera, J., Eregama, S., Gledhill, A., Petraglia, M.D., Lee-Thorpe, J.A., 2015b. Direct evidence for human reliance on rainforest resources in late Pleistocene Sri Lanka. Science 347 (6227), 1246–1249. https://doi.org/10.1126/science.aaa1230.
Roberts, P., Stewart, B.A., 2018. Defining the 'generalist specialist' niche for Pleistocene *Homo sapiens*. Nat. Human Behav. 2, 542–550. https://doi.org/10.1038/s41562-018-0394-4.
Rommerskirchen, F., Eglinton, G., Dupont, L., Güntner, U., Wenzel, C., Rullkötter, J., 2003. A north to south transect of Holocene southeast Atlantic continental margin sediments: relationship between aerosol transport and compound-specific $\delta^{13}C$ land plant biomarker and pollen records. G-cubed 4 (12). https://doi.org/10.1029/2003GC000541.
Rommerskirchen, F., Plader, A., Eglinton, G., Chikaraishi, Y., Rullkötter, J., 2006. Chemotaxonomic significance of distribution and stable carbon isotopic composition of long-chain alkanes and alkan-1-ols in C4 grass waxes. Org. Geochem. 37 (10), 1303–1332. https://doi.org/10.1016/j.orggeochem.2005.12.013.
Sage, R.F., 2017. A portrait of the C_4 photosynthetic family on the 50th anniversary of its discovery: species number, evolutionary lineages, and Hall of Fame. J. Exp. Bot. 68 (2), e11–e28. https://doi.org/10.1093/jxb/erx005.
Scerri, E.M.L., Roberts, P., Maezumi, Y., Malhi, Y., 2022. Tropical forests in the deep human past. Philosoph. Transac. Royal Soc. B 377 (1849). https://doi.org/10.1098/rstb.2020.0500.
Schuster, A.-C., Burghardt, M., Alfarhan, A., Bueno, A., Hedrich, R., Leide, J., Thomas, J., Reiderer, M., 2016. Effectiveness of cuticular transpiration barriers in a desert plant at controlling water loss at high temperatures. AoB Plants 8, 1–14.
Shackelford, L.L., Demeter, F., Westaway, K., Duringer, P., Ponche, J.-L., Sayavongkhamdy, T., Zhao, J.-X., Barnes, L., Boyon, M., Sichanthongtip, P., Sénégas, F., Patole-Edoumba, E., Coppens, Y., Dumoncel, J., Bacon, A.-M., 2018. Additional evidence for early modern human morphological diversity in Southeast Asia, at Tam Pa Ling, Loas. Quat. Int. 466, 93–106. https://doi.org/10.1016/j.quaint.2016.12.002. Part A.
Shipton, C., Roberts, P., Archer, W., Armitage, S.J., Bita, C., Blinkhorn, J., Courtney-Mustaphi, C., Crowther, A., Curtis, R., D' Errico, F., Douka, K., Faulkner, P., Groucutt, H.S., Helm, R., Herries, A.I.R., Jembe, S., Kourampas, N., Lee-Thorp, J., Marchant, R., Mercader, J., Marti, A.P., Prendergast, M.E., Rowson, B., Tengeza, A., Tibesasa, R., White, T.S., Petraglia, M.D., Boivin, N., 2018. 78,000-year-old record of Middle and later stone age innovation in an east african tropical forest. Nat. Commun. 9 (1832) https://doi.org/10.1038/s41467-018-04057-3.
Silvera, K., Neubig, K.M., Whitten, W.M., Williams, N.H., Winter, K., Cushman, J.C., 2010. Evolution along the crassulacean acid metabolism continuum. Funct. Plant Biol. 37 (11), 995–1110. https://doi.org/10.1071/FP10084.
Smith, F.A., Wing, S.L., Freeman, K.H., 2007. Magnitude of the carbon isotope excursion at the Paleocene-Eocene thermal maximum: the role of plant community change. Earth Planet Sci. Lett. 262 (1–2), 50–65. https://doi.org/10.1016/j.epsl.2007.07.021.
Still, C.J., Berry, J.A., Collatz, G.J., DeFries, R.S., 2003. Global distribution of C_3 and C_4 vegetation: carbon cycle implications. Global Biogeochem. Cycles 17 (1). https://doi.org/10.1029/2001GB001807.
Suraprasit, K., Shoocongdej, R., Chintakanon, K., Bocherens, H., 2021. Late Pleistocene human paleoecology in the highland savanna ecosystem of mainland Southeast Asia. Sci. Rep. 11, 16756 https://doi.org/10.1038/s41598-021-96260-4.
Sutikna, T., Tocheri, M.W., Morwood, M.J., Saptomo, E.W., Jatmiko, Due Awe, R., Westaway, K.E., Aubert, M., Li, B., Zhao, J-x., Alloway, B.V., Morley, M.W., Meijer, H.J.M., van den Bergh, G.D., Grün, R., Dosseto, A., Brumm, A., Jungers, W.L., Roberts, R., 2016. Revised stratigraphy and chronology for *Homo floresiensis* at liang bua, Indonesia. Nature 532, 366–369. https://doi.org/10.1038/nature17179.
Thomson, J.R., Holden, P.B., Anand, P., Edwards, N.R., Porchier, C.A., Harris, N.B.W., 2021. Tectonic and climate drivers of Asian monsoon evolution. Nat. Commun. 12 (4022) https://doi.org/10.1038/s41467-021-24244-z.
Tipple, B.J., Meyers, S.R., Pagani, M., 2010. Carbon isotope ratio of Cenozoic CO_2: a comparative evaluation of available geochemical proxies. Paleoceanogr. Paleoclimatol. 25 (3) https://doi.org/10.1029/2009PA001851.
Tipple, B.J., Pagani, M., 2007. The early origins of terrestrial C_4 photosynthesis. Annu. Rev. Earth Planet Sci. 35 (1), 435–461.

van der Merwe, N.J., Medina, E., 1991. The canopy effect, carbon isotope ratios and foodwebs in amazonia. J. Archaeol. Sci. 18 (3), 249–259. https://doi.org/10.1016/0305-4403(91)90064-V.

Vogel, J.C., 1978. Isotopic assessment of the dietary habits of Ungulates. South Afr. J. Sci. 74 (8). https://hdl.handle.net/10520/AJA00382353_9939.

Vogts, A., Moossen, H., Rommerskirchen, F., Rullkötter, J., 2009. Distribution patterns and stable carbon isotopic composition of alkanes and alkan-1-ols from plant waxes of African rain forest and savanna C_3 species. Org. Geochem. 40 (10), 1037–1054. https://doi.org/10.1016/j.orggeochem.2009.07.011.

Wang, B., 2006. The Asian Monsoon. Springer Science & Business Media.

Wang, P., Clemens, S., Beaufort, L., Braconnot, P., Ganssen, G., Jian, Z., Kershaw, P., Sarnthein, M., 2005. Evolution and variability of the Asian monsoon system: state of the art and outstanding issues. Quat. Sci. Rev. 24 (5–6), 595–629. https://doi.org/10.1016/j.quascirev.2004.10.002.

Wang, Y.J., Cheng, H., Edwards, R.L., An, Z.S., Wu, J.Y., Shen, C.-C., Dorale, J.A., 2001. A high-resolution absolute-dated late Pleistocene monsoon record from Hulu cave, China. Science 294 (5550), 2345–2348. https://doi.org/10.1126/science.1064618.

Wang, Y.J., Cheng, H., Edwards, R.L., Kong, X., Shao, X., Chen, S., Wu, J., Jiang, X., Wang, X., An, Z., 2008. Millennial-and orbital-scale changes in the East Asian monsoon over the past 224,000 years. Nature 451, 1090–1093. https://doi.org/10.1038/nature06692.

Webster, P.J., Magaña, V.O., Palmer, T.N., Shukla, J., Tomas, R.A., Yanai, M., Yasunari, T., 1998. Monsoons: processes, predictability, and the prospects for prediction. J. Geophys. Res. Oceans 103 (C7), 14451–14510. https://doi.org/10.1029/97JC02719.

Wedage, O., Picin, A., Blinkhorn, J., Douka, K., Deraniyagala, S., Kourampas, N., Perera, N., Simpson, I., Boivin, N., Petraglia, M., Roberts, P., 2019. Microliths in the south asian rainforest ~45-5 ka: new insights from fa-hien lena cave, Sri Lanka. PLoS One 14 (10). https://doi.org/10.1371/journal.pone.0222606.

Westaway, K.E., Louys, J., Due Awe, R., Morwood, M.J., Price, J.G., Zhao, J.-X., Aubert, M., Joannes-Boyau, R., Smith, T.M., Skinner, M.M., Compton, T., Bailey, R. M., van den Bergh, G.D., de Vos, J., Pike, A.W.G., Stringer, C., Saptomo, E.W., Rizal, Y., Zaim, J., Santoso, W.D., Trihascaryo, A., Kinsley, L., Sulistyanto, B., 2017. An early modern human presence in Sumatra 73,000-63,000 years ago. Nature 548, 322–325. https://doi.org/10.1038/nature23452.

Wu, M.S., Feakins, S.J., Martin, R.E., Shenkin, A., Bentley, L.P., Blonder, B., Salinas, N., Asner, G.P., Malhi, Y., 2017. Altitude effect on leaf wax carbon isotopic composition in humid tropical forests. Geochem. Cosmochim. Acta 206, 1–17. https://doi.org/10.1016/j.gca.2017.02.022.

Zech, M., Pedentchouk, N., Buggle, B., Leiber, K., Kalbitz, K., Marković, S.B., Glaser, B., 2011. Effect of leaf litter degradation and seasonality on D/H isotope ratios of n-alkane biomarkers. Geochem. Cosmochim. Acta 75 (17), 4917–4928. https://doi.org/10.1016/j.gca.2011.06.006.

Zheng, Z., Lei, Z.-Q., 1999. A 400,000 year record of vegetational and climatic changes from a volcanic basin, Leizhou Peninsula, southern China. Palaeogeogr., Palaeoclimatol., Palaeogeogr. 145 (4), 339–362. https://doi.org/10.1016/S0031-0182(98)00107-2.

Zhou, Y., Grice, K., Stuart-Williams, H., Farquhar, G.D., Hocart, C.H., Lu, H., Liu, W., 2010. Biosynthetic origin of the saw-toothed profile in $\delta^{13}C$ and $\delta^{2}H$ of *n*-alkanes and systematic isotopic differences between *n*-, *iso*- and *anteiso*-alkanes in leaf waxes of land plants. Phytochemistry 71 (4), 388–403. https://doi.org/10.1016/j.phytochem.2009.11.009.

Zilhão, J., 2012. Chapter 4 – personal ornaments and symbolism among the neanderthals. Dev. Quat. Sci. 16, 35–49. https://doi.org/10.1016/B978-0-444-53821-5.00004-X.